AGU PUBLICATIONS

JGR

Journal of Geophysical Research: Planets

RESEARCH ARTICLE

10.1002/2017JE005367

Key Points:
- Mercury's surface has 12–20% metallic phases produced by space weathering and graphite-induced smelting of boninitic and komatiitic lavas
- If smelting occurred, it would have produced substantial abundances of CO that may have facilitated explosive volcanic processes on Mercury
- The S and Fe abundances on the surface of Mercury are sourced from volcanic processes and indicate a mantle that is at IW −3.2 to −4.3

Correspondence to:
F. M. McCubbin,
francis.m.mccubbin@nasa.gov

Citation:
McCubbin, F. M., Vander Kaaden, K. E., Peplowski, P. N., Bell, A. S., Nittler, L. R., Boyce, J. W., … McCoy, T. J. (2017). A low O/Si ratio on the surface of Mercury: Evidence for silicon smelting? *Journal of Geophysical Research: Planets*, *122*, 2053–2076. https://doi.org/10.1002/2017JE005367

Received 12 JUN 2017
Accepted 24 SEP 2017
Accepted article online 29 SEP 2017
Published online 20 OCT 2017

A Low O/Si Ratio on the Surface of Mercury: Evidence for Silicon Smelting?

Francis M. McCubbin[1], Kathleen E. Vander Kaaden[2], Patrick N. Peplowski[3], Aaron S. Bell[4], Larry R. Nittler[5], Jeremy W. Boyce[1], Larry G. Evans[6], Lindsay P. Keller[1], Stephen M. Elardo[7], and Timothy J. McCoy[8]

[1]NASA Johnson Space Center, Houston, TX, USA, [2]Jacobs Technology, NASA Johnson Space Center, Houston, TX, USA, [3]The Johns Hopkins University Applied Physics Laboratory, Laurel, MD, USA, [4]Institute of Meteoritics, Department of Earth and Planetary Sciences, University of New Mexico, Albuquerque, NM, USA, [5]Department of Terrestrial Magnetism, Carnegie Institution of Washington, Washington, DC, USA, [6]Computer Science Corporation, Lanham-Seabrook, MD, USA, [7]Geophysical Laboratory, Carnegie Institution of Washington, Washington, DC, USA, [8]Department of Mineral Sciences, National Museum of Natural History, Smithsonian Institution, Washington, DC, USA

Abstract Data from the Gamma-Ray Spectrometer (GRS) that flew on the MErcury Surface, Space ENvironment, GEochemistry, and Ranging spacecraft indicate that the O/Si weight ratio of Mercury's surface is 1.2 ± 0.1. This value is lower than any other celestial surface that has been measured by GRS and suggests that 12–20% of the surface materials on Mercury are composed of Si-rich, Si-Fe alloys. The origin of the metal is best explained by a combination of space weathering and graphite-induced smelting. The smelting process would have been facilitated by interaction of graphite with boninitic and komatiitic parental liquids. Graphite entrained at depth would have reacted with FeO components dissolved in silicate melt, resulting in the production of up to 0.4–0.9 wt % CO from the reduction of FeO to Fe^0—CO production that could have facilitated explosive volcanic processes on Mercury. Once the graphite-entrained magmas erupted, the tenuous atmosphere on Mercury prevented the buildup of CO over the lavas. The partial pressure of CO would have been sufficiently low to facilitate reaction between graphite and SiO_2 components in silicate melts to produce CO and metallic Si. Although exotic, Si-rich metal as a primary smelting product is hypothesized on Mercury for three primary reasons: (1) low FeO abundances of parental magmas, (2) elevated abundances of graphite in the crust and regolith, and (3) the presence of only a tenuous atmosphere at the surface of the planet within the 3.5–4.1 Ga timespan over which the planet was resurfaced through volcanic processes.

1. Introduction

The MErcury Surface, Space ENvironment, GEochemistry, and Ranging (MESSENGER) spacecraft collected data that provided important insights into the structure, chemical makeup, and compositional diversity of Mercury (Solomon et al., 2001). The X-ray Spectrometer (XRS), Neutron Spectrometer (NS), and Gamma-Ray Spectrometer (GRS) that were aboard the MESSENGER spacecraft provided the first detailed chemical analyses of Mercury's surface. Among the many discoveries about Mercury made by MESSENGER, several surprising compositional characteristics of the surface were observed. These discoveries include elevated sulfur abundances (up to 4 wt %), elevated abundances of graphitic carbon (0–4.1 wt % across the surface with an additional 1–3 wt % graphite above the global average in low reflectance materials), low iron abundances (less than 2 wt %), and low oxygen abundances (O/Si weight ratio of 1.40 ± 0.03) (Evans et al., 2012; Nittler et al., 2011; Peplowski, Lawrence, Evans, et al., 2015; Peplowski et al., 2016; Weider et al., 2014). These exotic characteristics likely have important implications for the thermochemical evolution of Mercury and point to a planet that formed under highly reducing conditions (McCubbin et al., 2012; Namur, Charlier, et al., 2016; Namur, Collinet, et al., 2016; Zolotov et al., 2013).

The S and Fe abundances were used to constrain the oxygen fugacity (fO_2) of Mercurian magmas between 2.6 and 7.3 log units below the iron-wüstite (IW) buffer (McCubbin et al., 2012; Namur, Charlier, et al., 2016; Namur, Collinet, et al., 2016; Zolotov et al., 2013), which is lower than any of the other terrestrial planets in the solar system (Ehlmann et al., 2016; Sharp et al., 2013; Wadhwa, 2008). The upper range was constrained by assuming all Fe on the surface was FeO, which yielded fO_2 values ranging from 2.6 to 3.0 log units below IW (McCubbin et al., 2012). The lower end of this range was constrained by

experimental data on silicate-sulfide equilibria, which resulted in fO_2 values ranging from 4.5 to 7.3 log units below IW (McCubbin et al., 2012; Namur, Charlier, et al., 2016; Namur, Collinet, et al., 2016; Zolotov et al., 2013). The lower end of this range in fO_2 corresponds to maximum FeO abundances in silicate liquids of less than 0.8 wt % FeO (O'Neill & Eggins, 2002), which is equivalent to less than 0.62 wt % Fe. Given that the average abundance of Fe measured on the surface by GRS is approximately 1.5 wt % Fe (Weider et al., 2014), the lower estimates of fO_2 indicate that most of the Fe on the surface should be hosted by metallic phases or sulfides (Zolotov et al., 2013). The inference of low FeO abundances in silicate minerals on the surface is also supported by ground-based and MESSENGER ultraviolet-visible spectral (UV-VIS) reflectance data that do not exhibit 1 μm crystal field absorptions that could be attributed to FeO on any area of the surface >20 km across (Blewett et al., 1997; Blewett et al., 2013; Ernst et al., 2010; Holsclaw et al., 2010; Izenberg et al., 2014; Riner et al., 2010; Robinson & Taylor, 2001; Vilas, 1988). However, a downturn is observed in data from the MESSENGER Visible and Infrared Spectrometer (VIRS) at wavelengths less than ~0.36 μm in some pyroclastic deposits on Mercury, which is attributed to oxygen-metal charge transfer and is supportive of FeO abundances of up to several tenths of a weight percent (Goudge et al., 2014; Weider et al., 2016). Nonetheless, the source of Fe on the surface remains enigmatic, and the distribution of Fe and its correlation with surface features indicate that Fe is likely indigenous to Mercury (Weider et al., 2014; Weider et al., 2015).

The surface elemental composition of Mercury as determined by MESSENGER has been used to identify up to nine distinct geochemical terranes (Peplowski, Lawrence, Feldmanet, et al., 2015; Vander Kaaden et al., 2017; Weider et al., 2015). Additionally, numerous modeling and experimental efforts have been undertaken to infer the mineralogy and petrology of Mercurian lavas and surface materials (Charlier, Grove, & Zuber, 2013; Namur, Charlier, et al., 2016; Namur, Collinet, et al., 2016; Namur & Charlier, 2017; Stockstill-Cahill et al., 2012; Vander Kaaden et al., 2017; Vander Kaaden & McCubbin, 2015a; Vander Kaaden & McCubbin, 2016). However, all of these efforts have presumed the following valence states for each of the measured elements: Si^{4+}, Ti^{4+}, Al^{3+}, $Cr^{2+/3+}$, Fe^{2+}, Mn^{2+}, Mg^{2+}, Ca^{2+}, Na^{+}, K^{+}, S^{2-}, and Cl^{-}. Based on these valence assignments, cations are first charged balanced with the measured anions S^{2-} and Cl^{-}, and the remaining charge deficit is then balanced by the addition of O^{2-} until the bulk composition is electroneutral. The aforementioned valence state assignments include an implicit assumption that sufficient O is available (given that S and Cl are measured directly), but given the preponderance of evidence for highly reducing conditions on Mercury, the validity of this assumption is unknown. Moreover, the valence-assignment-derived compositions for the geochemical terranes yield O/Si weight ratios ranging from 1.61 to 1.84, which is substantially higher than the preliminary O/Si weight ratio of 1.40 ± 0.03 determined by the MESSENGER GRS instrument (Evans et al., 2012). Consequently, the aim of the present study is to reevaluate the O/Si ratio of Mercury's surface using the entire MESSENGER GRS data set to reassess its implications for the thermochemical evolution of Mercury, including the nature of its surface materials and the geologic processes by which they formed.

2. O/Si Ratio From MESSENGER GRS

Evans et al. (2012) reported an O/Si weight ratio of 1.40 ± 0.03 for the surface of Mercury based on data from the MESSENGER GRS, and they noted that this value was appreciably lower than both modeled O/Si ratios for Mercury and O/Si ratios of typical solar system materials (Figure 1), which are typically in the range of 1.7 and 2.3, between the values of pyroxene and olivine (Nittler et al., 2004). Evans et al. (2012) did not use this measurement to provide an abundance of oxygen for the surface of the planet because, at that time, no prior Gamma-Ray Spectrometer data set had been used to derive O abundances, and there were no Mercurian samples that could be used as a point of comparison to validate the measurement. Consequently, the puzzling result was not widely incorporated into geochemical models for Mercury's mineralogy or magmatic evolution.

Following publication of Evans et al. (2012), data acquired by the Dawn Gamma-Ray and Neutron Detector (GRaND) instrument were used to derive Fe/O (and Si/O) ratios for asteroid 4 Vesta, finding an excellent match to the howardite-eucrite-diogenite meteorites (Prettyman et al., 2012). Additionally, Peplowski, Bazell, et al. (2015) reanalyzed the Near Earth Asteroid Rendezvous (NEAR) GRS data and derived O ratios for asteroid 433 Eros that are consistent with the L and LL chondrites in agreement with conclusions

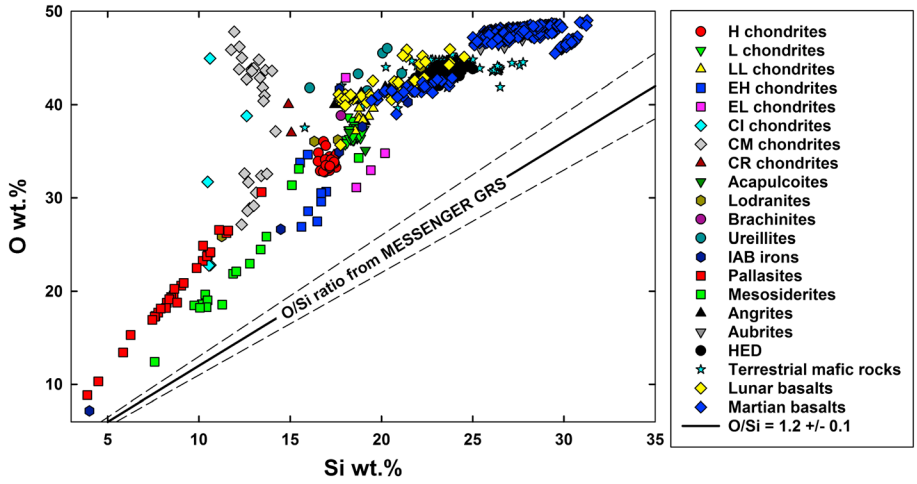

Figure 1. Plot of O abundance (wt %) versus Si abundance (wt %) for various chondrite and achondrite meteorites as well as mafic rocks from Earth, Moon, and Mars. A black line representing the measured O/Si weight ratio from MESSENGER GRS of 1.2 ± 0.1 is also displayed with the error envelope represented by a black dashed line. Data for the chondrite and achondrite meteorites were compiled from Nittler et al. (2004). Data from lunar samples were compiled from the Lunar Sample Compendium. Data from Mars were compiled from the Mars Meteorite Compendium as well as data from Aoudjehane et al. (2012) and Santos et al. (2015). Data from terrestrial rocks were downloaded from the PetDB (Lehnert et al., 2000) database (www.earthchem.org/petdb) on 8 September, 2017, using the following parameters: Data availability = major oxides and sample type = igneous:volcanic:mafic. Any terrestrial rocks with SiO_2 abundances greater than 60 wt % were excluded from the compilation.

drawn from other NEAR data sets that identified 433 Eros as an ordinary chondrite parent body. In light of these successful measurements, and following a detailed effort to validate neutron inelastic scattering cross sections for O to experimental data (Nelson et al., 2001), we have reevaluated and updated the MESSENGER-derived O/Si ratio to better understand its implications for the geochemistry, mineralogy, and petrology of Mercury's surface.

The analysis of the O/Si ratio determined here leverages the methodology of Evans et al. (2012) as well as the independent analysis techniques of Peplowski, Bazell, et al. (2015). The major improvement to our analysis is the recognition and removal of contribution from the 6,111 keV Cl gamma ray (Table 1; Evans et al., 2015) to the 6,129 keV O Gamma-Ray Peak analysis, which was not taken into account by Evans et al. (2012). To maximize the statistical precision of the measurement, all prime (Mercury-pointing, high quality) low-altitude (<2,000 km) data were used to create a summed spectra from which the 6,111 (Cl), 6,129 (O), and 1,778 (Si) keV Gamma-Ray Peaks were fitted to derive peak counting rates. These peak areas were compared with our modeled O and Si Gamma-Ray Count rates to yield a revised, northern hemisphere average O/Si weight ratio of 1.2 ± 0.1 (Table 2), which deviates substantially from the O/Si ratio of typical solar system materials (Figure 1). Direct comparisons of modeled and measured Mercury Gamma-Ray Spectra confirm that the 6,129 keV Gamma-Ray Flux is significantly (~30%) lower than expected. The error represents the one standard deviation statistical uncertainties in the measurement, as well as systematic uncertainties associated with various background corrections. We investigated the possibility of detecting spatial variations in O/Si ratios by binning GRS data acquired at high northern latitudes (e.g., primarily northern volcanic plains material), midnorthern and equatorial latitudes (primarily intercrater plains), and specifically within the "high-Mg region" as defined by MESSENGER XRS data (Weider et al., 2015). We observed no differences for any of these spatial regions at the one standard deviation level (Table 2).

Table 1
Results of Fits to the Oxygen and Silicon Peaks for a Summed Gamma-Ray Spectrum

			Count rate[a]	
	Element	Energy (KeV)	Low altitude	High altitude
Northern hemisphere	O	6,129	0.300 ± 0.011	0.065 ± 0.003
	Si	1,778	2.200 ± 0.022	0.197 ± 0.007

[a]Count rate and uncertainty in counts per minute.

The reevaluation of the O/Si ratio for the surface materials of Mercury indicates that the O/Si abundance is even lower than that reported in Evans et al. (2012), meaning that the O depletion relative to stoichiometric calculations of O abundances is even larger. This result indicates that the valence assignments of elements

Table 2
Oxygen Abundances for Selected Regions on Mercury

Spatial coverage	O/Si[a]	O wt %[b]
Northern Hemisphere	1.2 ± 0.1	29.5 ± 2.5

[a]O/Si weight ratio is derived from the count rates of Table 1 following Evans et al. (2012), including a "background amplification factor" of 1.49. Specifically, the Mercury originating signal is calculated as the low altitude count rate minus the high-altitude count rate × the background amplification factor. The ratio of the Si and O Mercury signals is divided by the ratio of the GRS efficiency for the two peaks (0.09/0.01) and then converted to an abundance ratio using Figure 2 of Peplowski et al. (2015). [b]Assuming a Si abundance of 24.6 wt %.

used in previous models for the composition of the surface have overestimated the abundance of O on Mercury. Using elemental compositions of the nine geochemical terranes that have been reported (Vander Kaaden et al., 2017; Weider et al., 2015), the overestimation of O is at a level of approximately 11–16 wt % O. This mismatch between the modeled and measured abundances of O on the surface has important implications for the geochemistry, mineralogy, and petrology of Mercury's surface. Likewise, if this O depletion is a primary geochemical feature, it could have important implications for the thermochemical evolution of Mercury's interior and the bulk composition of the planet.

3. Mechanisms for Balancing the Oxygen Deficit

The mismatch between the modeled and measured abundances of O on the surface of Mercury requires that the existing models be refined until they are consistent with the measurements. Previous studies that have aimed to determine the mineralogy and petrology of Mercury used the valence states discussed in section 1 to report surface and magma compositions in terms of oxides, sulfides, and chlorides (Charlier et al., 2013; Namur, Charlier, et al., 2016; Namur, Collinet, et al., 2016; Namur & Charlier, 2017; Stockstill-Cahill et al., 2012; Vander Kaaden et al., 2017; Vander Kaaden & McCubbin, 2015a; Vander Kaaden & McCubbin, 2016). Given that these models have overestimated the abundances of O, to make up for the deficit requires that some of the elements measured by GRS and XRS are not bonded to O^{2-}, S^{2-}, or Cl^{-}. Consequently, some of these elements are either bonded to different anions and/or some of the elements are themselves electroneutral and comprise metallic phases. Here we consider these two possibilities separately and evaluate the efficacy of each based on three criteria: (1) the cosmochemical abundances of the elements as depicted by their abundances in CI chondrites, (2) the stability of the resulting phases relative to the range of physical conditions (i.e., pressure, temperature, composition, and fO_2) experienced by Mercury, and (3) the composition of Mercury's surface as determined by MESSENGER.

3.1. Balancing the Oxygen Deficit With Anions

The first mechanism we consider for balancing the O deficit is to use O-free anions that were not considered in previous models. These anions could include C^{4-}, Si^{4-}, N^{3-}, P^{3-}, As^{3-}, Se^{2-}, Te^{2-}, H^{-}, F^{-}, Br^{-}, or I^{-}. This mechanism assumes that the valence assignments for the cations used in the previous studies were correct and that those cations are bonded to an anion other than oxygen that was not directly measured by MESSENGER. The exception to this assumption is Si^{4-}, which will be discussed later. Although instruments on the MESSENGER spacecraft were able to determine the abundances of many elements, they were unable to determine the ionic state of those elements. Furthermore, of the possible anion-forming elements listed, MESSENGER only provided data for Si (Evans et al., 2012; Nittler et al., 2011; Weider et al., 2015) and provided robust detection limits for C (Peplowski, Lawrence, Evans, et al., 2015), so we must evaluate the plausibility of many of the listed elements based on the computed elemental abundances and their typical cosmochemical abundances.

Table 3
Oxygen Deficit Due to Measured O/Si Ratio and Required Abundances of Other Anions to Accommodate the O Deficit of 11.5–15.8 wt % O

Element	Anion	Anion replacement factor[a]	Required abundance/ abundance in CI[b]
H	H^{-}	0.13	0.72–0.99
C	C^{4-}	0.38	1.25–1.72
N	N^{3-}	0.58	21.1–29.1
F	F^{-}	2.38	4,560–6,270
Si	Si^{4-}	0.44	0.48–0.65
P	P^{3-}	1.29	157–2,15
As	As^{3-}	3.12	194,000–267,000
Se	Se^{2-}	4.94	27,100–37,200
Br	Br^{-}	9.99	329,000–452,000
Te	Te^{2-}	7.98	400,000–549,000
I	I^{-}	15.86	4,250,000–5,840,000

[a]This factor is an intrinsic property of the atomic mass and charge of the anion that replaces O^{2-}. The factor is computed by dividing the required mass fraction of the element it would take to make up the entire O^{2-} deficit by the mass fraction of the O^{2-} deficit. [b]CI chondrite abundances were taken from Lodders and Fegley (1998).

The required abundance of each anion to balance the O deficit is computed by determining the abundance of that element, relative to oxygen, that is needed to satisfy the charge imbalance that is created by the O deficit. Each anion has a unique factor that we term an anion replacement factor, which is a function of the atomic mass and charge of the anion that replaces O^{2-}. Increasing atomic mass and decreasing negative charge relative to O^{2-} both increase the required abundance of an anion to make up for the O deficit. The anion replacement factors for all of the anions we considered are

listed in Table 3, along with the computed anion abundances relative to oxygen. We considered a computed anion abundance to be reasonable if it was within a factor of 15 of its abundance in CI chondrites because the abundances of the incompatible refractory trace elements Th and U are enriched on the surface of Mercury relative to CI chondrite by a factor of 7.6 ± 2 and 11.3 ± 2, respectively (Peplowski et al., 2011), and the moderately volatile incompatible elements Na, K, and Cl are enriched on the surface by a factor of 5.8 ± 0.2, 2.1 ± 0.4, and 2 ± 0.4 relative to CI chondrite, respectively (Evans et al., 2012; Evans et al., 2015; Peplowski et al., 2011). The abundances of each element that would be required to make up the O deficit are listed in Table 3. The abundances of N^{3-}, P^{3-}, As^{3-}, Se^{2-}, Te^{2-}, F^{-}, Br^{-}, and I^{-} required to make up the O deficit are exceedingly high relative to their abundances in CI chondrite (Table 3; Lodders, 2003; Lodders & Fegley, 1998), so we have dismissed these anions as a plausible means by which to make up the O deficit. The anions for which the computed elemental abundances in Table 3 were reasonable relative to their cosmochemical abundances include H^{-}, Si^{4-}, and C^{4-} (Lodders, 2003; Lodders & Fegley, 1998), so we will further assess their plausibility for making up the O deficit.

Based on the surface compositions determined by MESSENGER, the only potential cations of sufficient abundance to meaningfully contribute to making up the O deficit include Si^{4+}, Al^{3+}, Mg^{2+}, Fe^{2+}, Ca^{2+}, and Na^{+}. Consequently, we will only consider the stabilities of hydride, carbide, and silicide phases that contain the cations listed above. Furthermore, we will consider the stabilities of these phases relative to the equatorial daytime surface temperature on Mercury of 430°C (Vasavada et al., 1999) because latitudinal variations in the O/Si ratio were not observed, indicating that the primary phases controlling the O/Si ratio did not vaporize below 430°C. Of the potential hydride phases, iron hydride is not stable, SiH_4 is a gas above −112°C (silane), and AlH_3, MgH_2, and NaH breakdown to metal + H_2 gas at 150°C, 327°C, and 425°C, respectively (Lide, 2000). In fact, only CaH_2, with a decomposition temperature of 1000°C (Lide, 2000), is potentially stable under the surface conditions at Mercury. However, even if all Ca on the surface was converted to CaH_2, it would only equate to a total mass of 0.22–0.33 wt % H, but the total mass of hydrogen required to balance the O deficiency ranges from 1.45 to 2.00 wt % H. Consequently, hydrides are not a plausible anion to make up the O deficiency.

Carbides are refractory compounds that are stable at high temperatures, well in excess of 430°C (Lide, 2000), so the thermal stability of carbides will not hinder their ability to make up the O deficiency. In addition, carbon has been detected on the surface by the GRS and NS instruments that were on MESSENGER (Peplowski, Lawrence, Evans, et al., 2015; Peplowski et al., 2016). In fact, graphitic carbon is reported to be distributed globally on Mercury, possibly related to a primary graphite flotation crust (Peplowski et al., 2016; Vander Kaaden & McCubbin, 2015a). Graphite has also been proposed as a darkening agent on the surface of Mercury (Murchie et al., 2015) and has been linked to the formation of hollows (Blewett et al., 2016). Consequently, the inferred presence of carbon on the surface bolsters support for the possibility that carbides may be present. However, the total abundance of C in carbide phases required to make up the O deficiency is 4.3 to 6.0 wt % C. Data from the MESSENGER GRS instrument indicate that the surface abundance of C is 1.4 ± 0.9 wt % C; consistent with 0–4.1 wt % C at the three standard deviation level (Peplowski, Lawrence, Evans, et al., 2015). Consequently, carbides are a plausible mineral phase at the surface, but they cannot make up the entire O deficit.

The silicide anion is unique among the list of anions considered to make up the O deficit because it is also listed as a cation (Si^{4+}) that needs to be charge balanced. Furthermore, it is the only element on the list of anions for which we have an ample abundance at the surface of Mercury as determined by MESSENGER GRS and XRS data. However, there are some important limitations to consider, foremost of which is that silicon metal (Si^{0}) is not considered to be a silicide. Elemental silicon is a tetravalent metalloid, so it is discussed in section 3.2, which considers metallic phases for making up the O deficit. Furthermore, metalloids alloy with metals, so iron silicides are also considered in section 3.2. Therefore, here we only consider silicides of aluminum, magnesium, and calcium. Aluminum silicide decomposes above 167°C (Hentzell et al., 1987), so it is not a viable phase across the surface of Mercury. Although Mg_2Si and Ca_2Si are both stable above 430°C (Lide, 2000), they are unstable in the presence of SiO_2 because Mg_2Si and Ca_2Si both react with SiO_2 components to form MgO, CaO, and metallic Si^{0} (Ehrlich, 1963; Ropp, 2013). Consequently, the surface of Mercury has too much O to support the stability of Mg and Ca silicides. In summary, the O deficiency on Mercury cannot be reconciled by previously unaccounted anions, so balancing the O deficit requires that some of the presumed cations comprise metallic phases.

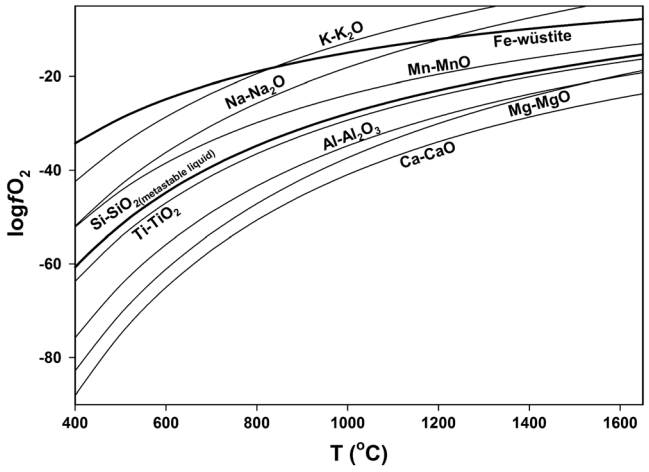

Figure 2. Plot of oxygen fugacity (fO_2) versus temperature (T) over the range of the equatorial daytime temperature on Mercury (430°C) and the estimated liquidus temperatures of the most refractory lavas on Mercury (1650°C; Namur, Charlier, et al., 2016). The solid black lines represent the oxygen fugacities of various metal-metal oxide reactions at 1 bar. The wüstite in the iron-wüstite reaction represents $Fe_{0.947}O$, and the SiO_2 in the Si-SiO_2 reaction represents a metastable SiO_2 melt. Thermodynamic data for all of the calculations obtained from JANAF tables (Chase, 1998).

3.2. Balancing the Oxygen Deficit With Metallic Phases

The second mechanism we consider for balancing the O deficit is to assume that certain elements that were assigned as cations in previous models are present on the surface as metallic phases. As stated in the previous section, the surface compositions determined by MESSENGER indicate that the only potential elements of sufficient abundance to meaningfully contribute to making up the O deficit include Si, Al, Mg, Fe, Ca, and Na, although we also consider K because the abundances on the surface have been determined. To differentiate between which of these elements are most likely to be in metallic phases and which are most likely to be bonded to oxygen on the surface of Mercury, we will examine the relative oxygen fugacities of the respective metal-metal oxide reactions for each of the listed elements over a range of relevant temperatures. The range of temperatures we have chosen is 430–1650°C. The lower end of this range was chosen because it represents the equatorial daytime temperature on the surface of Mercury (Vasavada et al., 1999), and 1650°C was chosen as the upper end of this range because it matches the liquidus temperatures of the most refractory surface terranes on Mercury (Namur, Collinet, et al., 2016). The results of our calculations are illustrated in Figure 2, and we have included information for additional common rock-forming elements (i.e., Mn and Ti) for comparison.

At 430°C, the relative stability of metal phases from most oxidizing to most reducing is Fe $\gg$ K $>$ Na $>$ Si $\gg$ Al $>$ Mg $>$ Ca. At 1650°C, the relative stability of metal phases is K $>$ Na $\gg$ Fe $\gg$ Si $>$ Mg $>$ Al $>$ Ca. Over the entire temperature range that we considered, Fe, K, Na, and Si are the most likely elements to constitute metallic phases, and of these, Si appears to be the least siderophile (Figure 2). As discussed previously, there is evidence for Fe comprising metallic phases on the surface; however, there is little-to-no evidence to suggest Na, K, and Si comprise metallic phases on Mercury. Although the computations illustrated in Figure 2 indicate that K and Na are stable metallic phases at higher oxygen fugacity than Si at 1 bar, experimental data indicate that Si is more siderophile than Na and K at low oxygen fugacity at elevated pressure (Namur, Collinet, et al., 2016; Vander Kaaden & McCubbin, 2016). In addition, Na, K, and Fe only account for a combined 8–17% of the O deficit, so Si metal must make up the bulk of the deficit regardless of whether or not the alkalis are hosted by metallic or nonmetallic phases. Nevertheless, the resulting mineralogy and petrology of the Mercurian surface is greatly affected by the hosting phases of the alkalis. Therefore, we will consider two end-member models, one that assumes all Na and K occur as monovalent cations (alkali-bearing bulk silicate) and one that assumes all Na and K are comprised of metallic phases (alkali-free bulk silicate). We consider both models to evaluate the surface composition and mineralogy of Mercury in light of the low O/Si ratio. However, we caution the reader that reality likely lies between the two end-member scenarios, so interpretations of this work resulting directly from the complete absence of alkalis in silicate phases or that requires the full accompaniment of alkalis in silicate phases should be avoided.

We assume for both models that all Fe on the surface of Mercury is hosted by metallic phases. The abundance of Fe metal in the nine terranes ranges from 0.9 to 2.0 wt % Fe, which can only account for 0.25–0.57 wt % O out of a deficit of 11.5–15.8 wt % O. In the alkali-bearing silicate model, the remainder of the O deficit is accounted for by 11.1–16.1 wt % metallic Si, which corresponds to 35–55% of the Si measured at the surface of Mercury being hosted by metallic phases. Given the propensity for alloying in the Fe-Si system (Hansen, 1958), it is likely that the Fe and Si metals occur as Fe-Si alloys. In the alkali-free silicate model, the abundance of Na metal in the nine terranes ranges from 3.0 to 5.4 wt % Na, and the abundance of K metal in the nine terranes ranges from 0.09 to 0.23 wt % K. Combined, Na and K only account for a combined 1.1–1.9 wt % O out of a deficit of 11.5–15.8 wt % O. Si metal is all that remains to make up the remainder of the deficit, equating to a range of 9.4–15.1 wt % Si metal in the nine geochemical terranes reported by Vander Kaaden et al. (2017). This range corresponds to 29–51% of the Si measured at the surface of Mercury being hosted in metallic phases.

4. Implications for the Mineralogy of the Surface of Mercury

The abundances of metallic phases needed to account for the low O/Si ratio at the surface of Mercury have important implications for the geochemistry, mineralogy, and petrology of the planet's surface. In particular, the oxide compositions of each of the geochemical terranes need to be reassessed and the normative mineralogy on the surface needs to be reevaluated. Additionally, the resulting oxide compositions of the terranes need to be assessed to determine whether or not the O/Si value that has been measured on the surface is a primary or secondary feature.

Previous studies have used MESSENGER data to predict the mineralogy at the surface of Mercury through modeling and experimental efforts (Charlier et al., 2013; Murchie et al., 2015; Namur, Charlier, et al., 2016; Namur, Collinet, et al., 2016; Namur & Charlier, 2017; Peplowski, Lawrence, Evans, et al., 2015; Peplowski et al., 2016; Stockstill-Cahill et al., 2012; Vander Kaaden et al., 2017; Vander Kaaden & McCubbin, 2015a; Vander Kaaden & McCubbin, 2016). The phases reported to occur on the surface include albitic plagioclase, enstatitic orthopyroxene, forsteritic olivine, diopside, silica, graphite, and Fe-, Ti-, Mn-, Ca-, and Mg-bearing sulfides (Charlier et al., 2013; Murchie et al., 2015; Namur, Charlier, et al., 2016; Namur, Collinet, et al., 2016; Namur & Charlier, 2017; Peplowski et al., 2016; Peplowski, Lawrence, Evans, et al., 2015; Stockstill-Cahill et al., 2012; Vander Kaaden et al., 2017; Vander Kaaden & McCubbin, 2015a; Vander Kaaden & McCubbin, 2016). In addition to these phases, alkali halides, orthoclase, kalsilite, and nepheline were also reported as potential minor components of the surface (Evans et al., 2015; Vander Kaaden et al., 2017). However, these studies did not take into account the low O/Si ratio on the surface, so we have reassessed the models of Mercury's mineralogy in light of the new O/Si data.

In the previous section, we determined the abundances of metallic phases that are required to match the observed O/Si weight ratio of 1.2 ± 0.1 using two end-member models identified as alkali-bearing silicate and alkali-free silicate. In the present section, we report the residual oxide compositions of the nine geochemical terranes from Vander Kaaden et al. (2017) after the metals are removed from the bulk compositions. We present two sets of compositions for each terrane with one representing all alkalis removed as metal (hereafter alkali-free bulk silicate composition) and another representing all alkalis retained as oxides (hereafter alkali-bearing bulk silicate compositions). Subsequently, we compute a CIPW norm (Cross et al., 1903) to determine the normative mineralogy for each composition, which we compare to the previously reported mineralogy.

The nine geochemical terranes identified by Vander Kaaden et al. (2017) include (i) the high-Mg region (HMR); (ii) a subregion of the HMR with the planet's highest Ca and S contents (HMR-CaS); (iii) a subset of the northern volcanic plains (NP) with relatively high Mg content (NP-HMg), distinguished by low-fast neutrons (Lawrence et al., 2017); (iv) a subset of the NP with relatively low Mg content (NP-LMg); (v) the Rachmaninoff basin (RB); (vi) the planet's largest pyroclastic deposit, located northeast of the Rachmaninoff basin (PD); (vii) the high-Al regions southwest and southeast of the NP (HAl); (viii) the smooth plains within the Caloris basin (CB); and (ix) the intermediate terrane (IT), composed of intercrater plains, highly cratered terrain, and the southern hemisphere. The metal-removed bulk silicate compositions for each of the nine geochemical terranes from Vander Kaaden et al. (2017) are reported in Tables 4 and 5.

We estimate a total potential range of 33–58 wt % SiO_2 across the silicate portion of Mercury's surface (Tables 4 and 5), which is more than twice as large as the range reported by Vander Kaaden et al. (2017). MgO abundances range from 16.0 to 37 wt % (Tables 4 and 5), which are enriched by more than a factor of 2 relative to the silicate compositions reported previously. CaO and Al_2O_3 are also enriched by more than a factor of 2 relative to the silicate compositions reported previously (Tables 4 and 5).

The elevated S abundances at the Mercurian surface coupled with the absence of Fe in the bulk silicate compositions require us to determine normative sulfide abundances and remove them from the bulk composition prior to computing the CIPW norm, similar to the calculations of Vander Kaaden et al. (2017). With the exception of minor Ti in the Caloris Basin, Mg, and Ca are the most chalcophile elements that remained in the bulk silicate compositions (Vander Kaaden & McCubbin, 2016). Consequently, MgS and CaS were determined to be the sulfide phases to remove from the bulk compositions, although we first removed 0.75 wt % TiS_2 from the CB composition before removing MgS and CaS. To execute this calculation, we used a sulfide melt Ca-Mg exchange coefficient of 1.97 (Vander Kaaden & McCubbin, 2016), and we removed the two sulfide phases until all the S was consumed. This removal resulted in a modal range of 1.1–5.5 wt % MgS and 0.17–0.84 wt % CaS in the bulk compositions of the nine geochemical terranes (Tables 6 and 7).

Table 4
Average Compositions (Wt %) for Bulk Silicate Portion of Nine Distinct Geochemical Regions on Mercury Reported by Vander Kaaden et al. (2017) With Appropriate Fe, Na, K, and Si Metal Components Removed to Account for Measured O/Si Ratio

	HMR	HMR-CaS	CB	NP-HMg	NP-LMg	RB	HAl	PD	IT
SiO_2	38.33	36.30	49.33	43.49	57.80	39.34	42.82	38.49	45.04
TiO_2	0.00	0.00	0.64	0.00	0.00	0.00	0.00	0.00	0.00
Al_2O_3	14.54	13.50	22.93	18.02	16.39	15.06	23.96	17.43	19.95
MgO	34.94	36.61	18.04	29.07	16.85	33.75	23.56	32.43	25.45
FeO	0.00	0.00	0.00	0.00	0.00	0.00	0.00	0.00	0.00
CaO	10.13	11.30	7.88	8.00	7.32	9.86	8.18	11.09	8.14
Na_2O	0.00	0.00	0.00	0.00	0.00	0.00	0.00	0.00	0.00
K_2O	0.00	0.00	0.00	0.00	0.00	0.00	0.00	0.00	0.00
S	3.86	4.31	2.10	2.58	2.53	3.70	2.68	0.85	2.57
Cl	0.17	0.17	0.17	0.17	0.47	0.17	0.17	0.18	0.17
−O = S	1.97	2.19	1.09	1.33	1.37	1.89	1.38	0.46	1.32
Total	100.00	100.00	100.00	100.00	100.00	100.00	100.00	100.00	100.00
Mg/Si (Wt)	1.18	1.30	0.47	0.86	0.38	1.11	0.71	1.09	0.73
Al/Si (Wt)	0.43	0.42	0.53	0.47	0.32	0.43	0.63	0.51	0.50
$\Delta T_{KVK2017}$ (°C)[a]	173	182	−87	180	−92	180	91	302	74

[a]Difference between the liquidus temperature calculated with MAGPOX (i.e., Davenport et al., 2014 ; Longhi, 1991, 1992) for a given terrane composition in the present study and the corresponding terrane composition reported in Vander Kaaden et al. (2017).

The results of our alkali-free bulk silicate CIPW norm calculations are provided in Table 6, and the results of our alkali-bearing bulk silicate CIPW norm calculations are provided in Table 7. Pie charts illustrating the results from Tables 6 and 7 are presented in Figures 3 and 4, respectively. In order to compute the CIPW norms for several of the bulk silicate compositions, we needed to include a normative periclase (MgO) component because they contained excess MgO. Additionally, five of the geochemical terranes had normative corundum (Al_2O_3). In cases where a composition had both normative periclase and normative corundum, we added a spinel ($MgAl_2O_4$) component until either periclase or corundum was consumed. Additionally, we attributed all Cl in the terranes to $CaCl_2$, but it could be hosted by other halides.

The results of the alkali-free bulk silicate CIPW norm indicate that all compositions have either normative periclase or normative corundum. The periclase normative terranes (HMR, HMR-CaS, RB, and PD) are highly silica undersaturated and have normative larnite (Ca_2SiO_4). All of the terranes with normative corundum (CB, NVP-HMg, NVP-LMg, Hal, and IT) are also hypersthene normative (i.e., contains normative enstatite $MgSiO_3$), and two of those terranes (CB and NVP-LMg) have normative quartz (SiO_2). With the exception of CB and

Table 5
Average Compositions (wt %) for Bulk Silicate Portion of Nine Distinct Geochemical Regions on Mercury Reported by Vander Kaaden et al. (2017) With Appropriate Fe and Si Metal Components Removed to Account for Measured O/Si Ratio

	HMR	HMR-CaS	CB	NP-HMg	NP-LMg	RB	HAl	PD	IT
SiO_2	34.83	32.83	45.75	39.81	51.11	35.82	39.24	34.89	41.47
TiO_2	0.00	0.00	0.62	0.00	0.00	0.00	0.00	0.00	0.00
Al_2O_3	14.15	13.13	22.36	17.52	15.66	14.66	23.32	16.94	19.43
MgO	33.99	35.61	17.59	28.27	16.10	32.84	22.93	31.53	24.79
FeO	0.00	0.00	0.00	0.00	0.00	0.00	0.00	0.00	0.00
CaO	9.85	10.99	7.68	7.78	6.99	9.59	7.96	10.78	7.93
Na_2O	4.94	4.97	4.73	4.89	8.33	4.92	4.88	5.07	4.85
K_2O	0.23	0.23	0.12	0.33	0.23	0.22	0.22	0.23	0.15
S	3.76	4.19	2.05	2.51	2.42	3.60	2.61	0.82	2.50
Cl	0.17	0.17	0.16	0.17	0.45	0.17	0.17	0.17	0.17
−O = S + Cl	1.91	2.13	1.06	1.29	1.31	1.84	1.34	0.45	1.29
Total	100.00	100.00	100.00	100.00	100.00	100.00	100.00	100.00	100.00
Mg/Si (Wt)	1.26	1.40	0.50	0.92	0.41	1.18	0.75	1.17	0.77
Al/Si (Wt)	0.46	0.45	0.55	0.50	0.35	0.46	0.67	0.55	0.53
$\Delta T_{KVK2017}$ (°C)[a]	343	401	−29	310	−74	340	212	470	175

[a]Dfference between the liquidus temperature calculated with MAGPOX (i.e., Davenport et al., 2014 ; Longhi, 1991, 1992) for a given terrane composition in the present study and the corresponding terrane composition reported in Vander Kaaden et al. (2017).

Table 6
CIPW Norm for Each of the Nine Distinct Geochemical Regions on Mercury Reported by Vander Kaaden et al. (2017), Assuming the Presence of Fe, Na, K, and Si Metal to Account for the Measured O/Si Ratio

Mineral group	Phase	HMR	HMR-CaS	CB	NP-HMg	NP-LMg	RB	HAl	PD	IT
Silicates	Anorthite	32.00	29.47	30.49	30.09	26.25	33.30	30.52	37.81	30.65
	Quartz	-	-	7.75	-	19.42	-	-	-	-
	Hypersthene	-	-	33.92	22.06	29.35	-	31.34	-	33.23
	Forsterite	39.08	35.58	-	21.67	-	40.55	7.47	32.59	9.01
	Larnite	1.66	3.63	-	-	-	0.98	-	1.48	-
Oxides	Periclase	2.46	5.51	-	-	-	0.78	-	6.50	-
	Corundum	-	-	7.96	3.64	4.07	-	8.45	-	5.12
Metals	Fe	1.81	2.00	0.89	1.83	1.42	1.77	0.88	1.83	1.67
	Si	13.88	14.05	12.51	13.40	9.39	13.75	13.92	15.09	13.14
	Na	3.05	3.06	3.01	3.04	5.41	3.05	3.05	3.09	3.03
	K	0.16	0.16	0.09	0.23	0.17	0.16	0.16	0.16	0.11
Halides	$CaCl_2$	0.22	0.22	0.22	0.22	0.62	0.22	0.22	0.22	0.22
Sulfides	MgS	4.97	5.48	2.01	3.36	3.23	4.77	3.42	1.06	3.31
	CaS	0.71	0.84	0.42	0.45	0.68	0.68	0.58	0.17	0.52
	TiS_2	-	-	0.75	-	-	-	-	-	-

Note. Phase abundances expressed in weight percent.

NVP-LMg, all of the terranes have normative forsterite (Mg_2SiO_4), and all of the terranes have normative anorthite ($CaAl_2Si_2O_8$).

The results of the alkali-bearing bulk silicate CIPW norm indicate that all compositions are nepheline ($NaAlSiO_4$) normative, so they are all silica undersaturated. Moreover, six of the terranes (HMR, HMR-CaS, NVP-HMg, RB, HAl, and PD) have normative periclase, and with the exception of HAl, all of the periclase-bearing terranes have normative larnite. All of the terranes have normative forsterite and normative anorthite. Two of the terranes (NVP-HMg and IT) have normative diopside ($CaMgSi_2O_6$), and two of the terranes (CB and NVP-LMg) have normative albite ($NaAlSi_3O_8$). The alkali-bearing bulk silicate CIPW norm also indicates a number of minor phases, including corundum, spinel, orthoclase ($KAlSi_3O_8$), and kalsilite ($KAlSiO_4$).

All of the minerals predicted to occur on the surface of Mercury from previous studies that did not consider the measured O/Si ratio are represented in the updated normative mineralogy calculations from the present study. However, the relative abundances of the phases in each terrane have changed substantially from those reported in previous studies, so any existing mineral maps for the surface that were derived without accounting for the measured O/Si ratio likely require substantial modifications and updates. In addition to the minerals previously reported to occur on Mercury, we suggest that several additional phases be considered based on our CIPW norm calculations, including metallic Si, Fe, Na, and K, periclase, anorthitic plagioclase, corundum, spinel, and larnite, although larnite would likely exist as monticellite or a larnite component in forsterite. Furthermore, the albite and anorthite components likely constitute a single plagioclase phase. In summary, when the measured O/Si ratio is taken into consideration, the prospects for mineralogical diversity across the Mercurian surface increases substantially. However, we caution the reader that CIPW norm calculations (i.e., Tables 6 and 7) are used here as a guide, and we do not intend for it to represent an accurate predictor of the actual modal mineralogy on the surface of Mercury.

5. Is the O/Si Ratio of Mercury's Surface a Primary Feature?

Whether the low O/Si ratio of the surface is a primary or secondary feature has profound implications for the thermochemical evolution of Mercury. However, we must first define what is implied by the terms primary feature and secondary feature. The O/Si ratio of a surface composition is considered to be a primary feature if that ratio has either remained unmodified or has only been modified by fractional crystallization processes since the time that the materials left the mantle source region and were erupted onto the surface. The O/Si ratio of a Mercurian surface composition is considered to be a secondary feature if that ratio has been modified by secondary processes such as space weathering, impact processing, magmatic degassing, or crustal assimilation. In this section, we consider only the

Table 7
CIPW Norm for Each of the Nine Distinct Geochemical Regions on Mercury Reported by Vander Kaaden et al. (2017), Assuming the Presence of Fe and Si Metal to Account for the Measured O/Si Ratio

Mineral group	Phase	HMR	HMR-CaS	CB	NP-HMg	NP-LMg	RB	HAl	PD	IT
Silicates	Anorthite	12.99	10.48	29.83	20.80	3.89	14.31	30.49	18.59	25.92
	Albite	-	-	17.30	-	26.73	-	-	-	0.05
	Orthoclase	-	-	0.63	-	1.18	-	-	-	0.76
	Diopside	-	-	-	-	17.22	-	-	-	3.67
	Forsterite	29.29	25.88	23.79	35.63	14.97	30.75	27.67	22.84	31.12
	Larnite	7.46	9.41	-	2.85	-	6.80	-	7.41	-
	Nepheline	18.67	18.58	9.54	18.70	19.00	18.66	18.77	18.99	18.69
	Kalsilite	0.63	0.63	-	0.93	-	0.62	0.61	0.64	-
Oxides	Periclase	8.40	11.46	-	0.86	-	6.72	0.40	12.18	-
	Corundum	-	-	1.18	-	-	-	-	-	-
	Spinel	-	-	-	-	-	-	2.08	-	-
Metals	Fe	1.81	2.00	0.89	1.83	1.42	1.77	0.88	1.83	1.67
	Si	14.84	15.01	13.44	14.38	11.08	14.71	14.88	16.06	14.09
Halides	$CaCl_2$	0.22	0.22	0.22	0.22	0.62	0.22	0.22	0.22	0.22
Sulfides	MgS	4.97	5.48	2.01	3.36	3.22	4.77	3.42	1.06	3.31
	CaS	0.71	0.84	0.42	0.45	0.68	0.68	0.58	0.17	0.52
	TiS_2	-	-	0.75	-	-	-	-	-	-

Note. Phase abundances expressed in weight percent.

implications of the O/Si ratio being a primary feature, and we consider the possibility that it is a secondary feature in a subsequent section.

Volcanic processes resurfaced Mercury approximately 4.0–4.1 Ga (Marchi et al., 2013) and volcanic processes largely ceased by about 3.5 Ga (Byrne et al., 2016), leaving a crust that formed from volcanism exposed at the surface. If the O/Si weight ratio of 1.2 ± 0.1 determined by MESSENGER GRS is a primary feature, it would imply that the erupted volcanic products also had this ratio. Furthermore, these volcanic products would have to be a mixture of silicate melt and approximately 12–20 wt % primary metallic components, all of which have a much greater density than the melts in which they would be entrained Vander Kaaden and McCubbin (2015a). The silicate compositions are also highly exotic with excessive normative corundum (Table 6) or extreme silica undersaturation as evidenced by normative nepheline and normative periclase (Tables 6 and 7). Furthermore, if the O/Si ratio represents a primary feature of the planet's mantle, it would indicate that the planet did not fully differentiate given that Mercury would host 12–20% (or more) primary metallic components in the silicate mantle, which is inconsistent with the past presence of a magma ocean on Mercury (Brown & Elkins-Tanton, 2009; Riner et al., 2009; Vander Kaaden & McCubbin, 2015a) where silicate and metal would have been separated into a silicate mantle and a metallic core. Given the improbable likelihood of meeting the prerequisites required to declare that the O/Si ratio represents a primary feature of volcanic products erupted onto the surface, we disfavor a primary origin for the low O/Si ratio of Mercury's surface and explore the possibility of it being related to a secondary process.

6. Secondary Processes That Could Have Affected the O/Si Ratio of Mercury's Surface

By attributing the low O/Si ratio of Mercury's surface to a secondary process, we are limiting the process to one that either adds metals to the surface or one that causes the loss of oxygen from the surface. However, we do not consider processes that add metal/carbides to the surface through exogenic sources because the chemical variations across the surface do not correlate to variations in the O/Si ratio (Weider et al., 2014), and there is not a plausible source of material in the solar system that would add substantial amounts of carbides or Si-rich metals to the surface of Mercury. Consequently, we will consider only O-loss processes. Of the processes that can cause the loss of O, we consider space weathering and magmatic degassing (from lavas or impact melts) because both processes can lead to the loss of oxygen species (Fogel & Rutherford, 1995; Hapke, 2001; Keller & McKay, 1997; Lucey & Riner, 2011; Noble et al., 2005; Noble & Pieters, 2003; Pieters et al., 2000; Rutherford & Papale, 2009; Sharp et al., 2013; Sato, 1979; Zolotov, 2011).

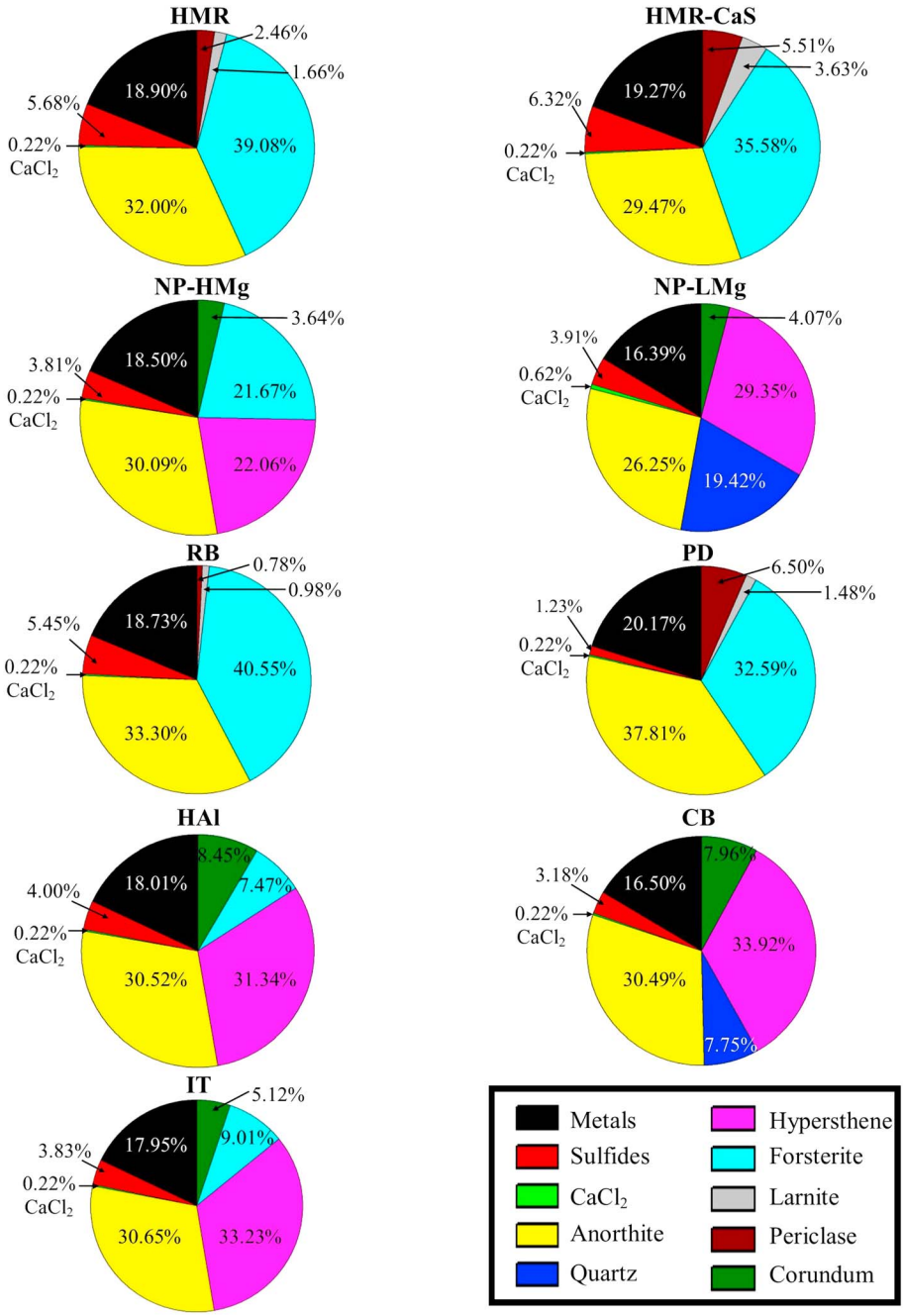

Figure 3. Results of the CIPW normative calculations for each of the nine geochemical regions using the alkali-free bulk silicate compositions from Table 4. See Table 6 for the tabulated CIPW norm values depicted in the pie charts above.

6.1. Space Weathering as a Mechanism to Lose Oxygen on Mercury

Space weathering is the gradual alteration of surface materials on airless bodies that occurs during exposure to the space environment. Space weathering is typically grouped into two categories, including (1) micrometeorite impacts and (2) irradiation (from the Sun, high-energy galactic cosmic rays, or the magnetosphere) (Pieters & Noble, 2016). Much of what is known about space weathering products was realized through the study of lunar samples. Based on lunar sample studies, one of the primary metallic byproducts of space weathering is iron metal (Keller & McKay, 1993; Keller & McKay, 1997; Noble et al., 2001; Taylor et al., 2001), although iron silicides (e.g., hapkeite) and rare metallic Si also make up a minor fraction of metallic space weathering

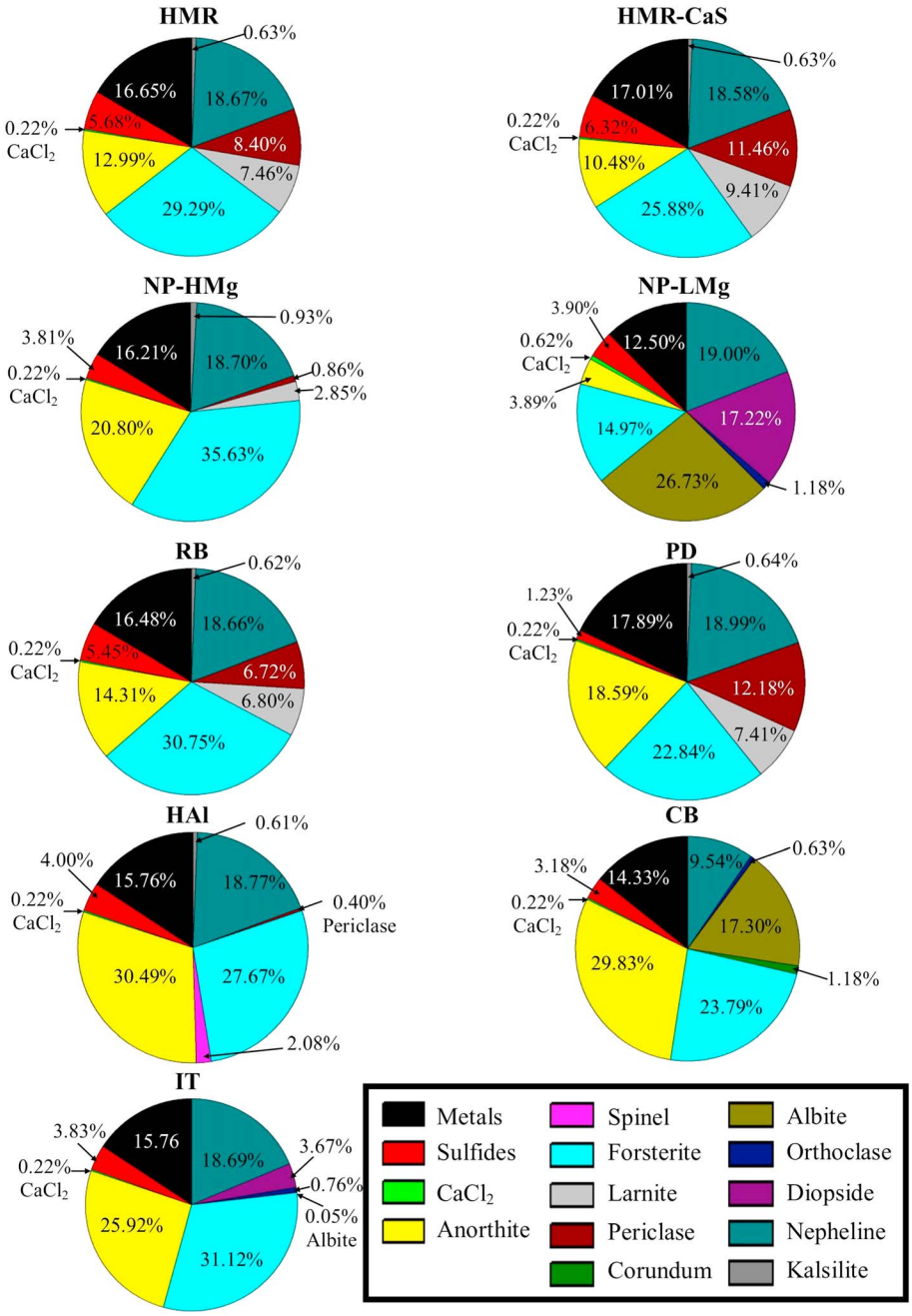

Figure 4. Results of the CIPW normative calculations for each of the nine geochemical regions using the alkali-bearing bulk silicate compositions from Table 5. See Table 7 for the tabulated CIPW norm values depicted in the pie charts above.

products (Anand et al., 2004; Gopon et al., 2017). The iron metal produced through space weathering occurs along a continuum of nanophase iron particles that coarsen through Ostwald ripening to larger particles (Lucey & Noble, 2008; Noble et al., 2007; Pieters et al., 2000; Pieters & Noble, 2016). In addition to metal particles, sulfides and halides have also been reported to form through space weathering processes based on studies of samples returned from the asteroid Itokawa by the Hayabusa spacecraft (Noguchi et al., 2011; Noguchi, Kimura, Hashimoto, Konno, Nakamura, Zolensky, Okazaki, & Ishibashiet, 2014a; Noguchi, Kimura, Hashimoto, Konno, Nakamura, Zolensky, Tsuchiyama, & Okadaet, 2014b).

The space weathering environment at Mercury is expected to be among the most extreme in the solar system given its proximity to the Sun and its mass relative to other airless bodies, both of which are expected to

enhance the speed and flux of impactors and the intensity of solar irradiation (Borin et al., 2009; Cintala, 1992; Domingue et al., 2014; Marchi et al., 2009). In comparison to the lunar regolith, the ratio of larger particles to smaller nanophase iron particles is expected to be substantially higher on Mercury as a consequence of the extreme space weathering environment (Lucey & Riner, 2011; Noble & Pieters, 2003), which is supported by the optical characteristics of Mercury's surface (Riner & Lucey, 2012). However, the abundance of Fe at Mercury's surface is insufficient to account for the amount of oxygen that was lost through the production of Fe metal alone. Even if all the Fe on Mercury was originally FeO that converted to Fe metal through space weathering, it would only account for 0.25–0.57 wt % O. Although iron silicides and metallic Si make up a minor volume fraction of space weathering products in lunar samples (Anand et al., 2004; Gopon et al., 2017), Gopon et al. (2017) report that the presence of trace amounts of reduced carbon in the lunar regolith may have aided in the production of iron silicides and metallic Si produced by space weathering. Consequently, the apparently graphite-rich nature of the Mercurian regolith and the extreme space weathering environment on Mercury both support the possibility that space weathering is a viable process by which oxygen could have been lost from a physicochemical standpoint. However, mass constraints on the loss of O via space weathering must be considered to fully evaluate the efficacy of this process as an O-loss mechanism on Mercury.

The MESSENGER GRS data on which our O/Si ratio is based provide chemical information on the upper ten to several tens of centimeters of the surface of Mercury (Solomon et al., 2001). In contrast, metallic space weathering products typically form in the outer hundreds of nanometers of an exposed particle (Keller & McKay, 1993; Keller & McKay, 1997; Noble et al., 2001; Pieters & Noble, 2016; Pieters et al., 2000; Taylor et al., 2001). The contrast in scales of the space weathering process and the GRS analysis requires that we consider the volume of material from which O has been lost and how it relates to mass. Consequently, we wish to consider the total mass of O lost from gardened regolith and compare it to the observed O deficit on Mercury. Because we do not have samples of Mercury's regolith, we have chosen to assess the mass fraction of O that is lost in the gardened lunar regolith as an analog. The lunar regolith is used as an analog for two primary reasons: (1) The mass fraction of Fe metal in the lunar regolith has been measured, so we can calculate the mass fraction of O that could have been yielded through the production of metal during space weathering, and (2) the abundance of FeO in the lunar regolith is not a limiting factor to the production of Fe metal, so it provides us with the limitations of O loss through regolith gardening. The average abundance of Fe metal in the lunar regolith that can be attributed to space weathering ranges from 0.7 to 1.0 wt % Fe^0 (Morris, 1980), which would only account for 0.20–0.29 wt % O, far less than the required 11.5–15.8 wt % O needed to account for the measured O/Si ratio on Mercury. Consequently, we infer that the process of regolith gardening is an important limiting factor in the efficiency of O loss from planetary surfaces by space weathering processes. Although the lunar analog indicates that space weathering cannot be the primary mechanism responsible for the low O/Si ratio on Mercury, the space weathering environment on Mercury is more intense than on the Moon, so the efficiency of O loss may be much greater on Mercury. Additional studies are needed to fully characterize the intensity of space weathering on Mercury and its implications for the amount of O loss that could occur through space weathering processes; however, we can conclude that space weathering likely contributed to the loss of O from Mercury surface materials.

6.2. Magmatic Degassing as an Oxygen-Loss Mechanism on Mercury

The loss of oxygen-bearing vapor species from lavas on Mercury represents another potential mechanism to lose O from the surface. The loss of vapor species from lavas and magmas is referred to as magmatic degassing, and the degassed constituents can be comprised of any number of magmatic volatile elements (H, C, N, O, F, S, Cl, noble gases, etc.). Magmatic degassing typically refers to the exsolution of fluid or vapor constituents that were dissolved in a silicate melt. These volatiles could have been incorporated into a silicate melt as early as the time of partial melting in the source, or they could have been dissolved into the melt through assimilation processes at any point along the liquid line of descent. Exsolution of a fluid or vapor phase from a silicate melt occurs when a volatile constituent exceeds its solubility in the silicate melt, which could occur at any point along the liquid line of descent, and commonly occurs due to changes in pressure, temperature, oxygen fugacity, melt composition, or abundance (e.g., crystallization of volatile-free minerals results in elevated abundances of the volatile element in the residual silicate melt) (Burnham, 1994; Carroll & Webster, 1994; Dixon & Stolper, 1995; Dixon et al., 1995; Holloway & Jakobsson, 1986; Jambon, 1994; Ustunisik et al.,

2015). Alternatively, magmas can undergo solid-liquid or solid-solid reactions that produce vapor phases as a byproduct with minimal dissolution of volatiles into the silicate melt. We will consider the former process here and the latter process in the following section.

The primary O-bearing magmatic volatile species on Earth occur in the C-O-H system (O_2, H_2O, H_2, CO_2, CO, and CH_4), which dominates the volatile budget of the silicate Earth (Dasgupta & Hirschmann, 2010; Jambon, 1994; Mysen et al., 2009). Of the gases considered in the C-O-H system, we focus only on the species that contain O, including O_2, H_2O, CO, and CO_2. Furthermore, we evaluate the solubility and speciation of C-O and O-H species in silicate liquids under the physical conditions afforded by Mercury to understand the plausibility of magmatic degassing as a mechanism to explain the low O/Si ratio. The highly reducing conditions on Mercury have important implications for the stable gas species that would evolve from Mercurian lavas. Under reducing conditions of three to seven log units below the IW buffer, options are limited because the partial pressure of O_2 in equilibrium with lavas at Mercurian fO_2 is exceedingly low (maximum of 10^{-14} bar O_2; Figure 2). At mantle pressures (>1 GPa), the solubility of H in silicate liquids is not markedly lower under highly reducing conditions compared to oxidizing conditions: however, the speciation of H is affected by oxygen fugacity (i.e., the H_2/H_2O abundance ratio is proportional to the fH_2/fH_2O ratio; Hirschmann et al., 2012). It also follows that H_2O would be a very minor vapor species in favor of H_2 given the relationship between fH_2/fH_2O ratios and oxygen fugacity (Hirschmann et al., 2012; Newcombe et al., 2017; Sharp et al., 2013; Zolotov et al., 2013). In fact, the preferential loss of H_2 from H-rich reduced magmas could lead to oxidation of the melt (Sharp et al., 2013), which would work against stabilizing metallic Fe or Si. Furthermore, carbon solubility in silicate liquids under such reducing conditions is severely limited (<1 ppm C; Eggler et al., 1979; Hirschmann & Withers, 2008; Li et al., 2017; Stanley et al., 2011; Stanley et al., 2012; Yoshioka et al., 2015). In summary, it is highly unlikely that the low O/Si ratio can be explained by magmatic degassing of C-O-H vapor species that were dissolved within Mercurian magmas. Although the surface is rich in sulfur, we did not consider degassing of S-O species to account for the loss of O because S-O species can make up only trace components relative to the dominance of sulfide species under Mercurian oxygen fugacities (Zolotov, 2011), and hence, degassing of S-O species cannot account for the low O/Si ratio.

6.3. Graphite-Induced Smelting as a Mechanism to Lose Oxygen on Mercury

Although solubilities of species in the C-O and O-H systems in silicate liquids is limited under Mercurian fO_2 (Li et al., 2017), there is evidence for a primary graphite flotation crust on Mercury (Peplowski et al., 2016; Vander Kaaden & McCubbin, 2015a), and additional evidence that graphite is present within the regolith (Murchie et al., 2015; Peplowski, Lawrence, Evans, et al., 2015). Consequently, graphite could be assimilated by Mercurian magmas during ascent through the primary crust or by lavas as they flowed across the graphite-bearing surface. The presence of graphite in Mercurian lavas provides a potential mechanism to produce O-bearing vapor species without the need for those species being dissolved in the silicate melt. Graphite is commonly used in industry for the formation of metals because it strips oxygen from other compounds (Bafghi et al., 1993; Bafghi et al., 1992; Miller et al., 1979; Sarma et al., 1996). This process of metal formation through the reaction of molten oxides with graphite is known as smelting. Smelting processes are not limited to anthropogenic influence. In fact, there are several examples of naturally occurring smelting processes that have occurred on Earth (Disko Island, Greenland; Northern Siberia, Russia; and Kassel, Germany; Bird & Weathers, 1977; Iacono-Marziano et al., 2012; Melson & Switzer, 1966; Pernet-Fisher et al., 2017; Ulffmoller, 1990), and smelting has also been invoked to explain the petrologic history of the parent body of the unusual ureilite meteorites (Goodrich et al., 2007; Singletary & Grove, 2003; Walker & Grove, 1993).

To assess the plausibility of smelting on Mercury, we consider the chemical reactions that would need to occur in order to form Fe, K, Na, and Si metal, which are the four elements that were determined to be the most susceptible to reduction in high temperature systems on Mercury (Figure 2). At the liquidus temperatures for Mercurian magmas, graphite hosted by lavas would react with melt species to form CO through the following reactions:

$$C_{graphite} + FeO_{melt} \longleftrightarrow CO_{gas} + Fe^0{}_{metal} \quad (1)$$

$$C_{graphite} + K_2O_{melt} \longleftrightarrow CO_{gas} + 2K^0{}_{gas} \quad (2)$$

$$C_{graphite} + Na_2O_{melt} \longleftrightarrow CO_{gas} + 2Na^0{}_{gas} \quad (3)$$

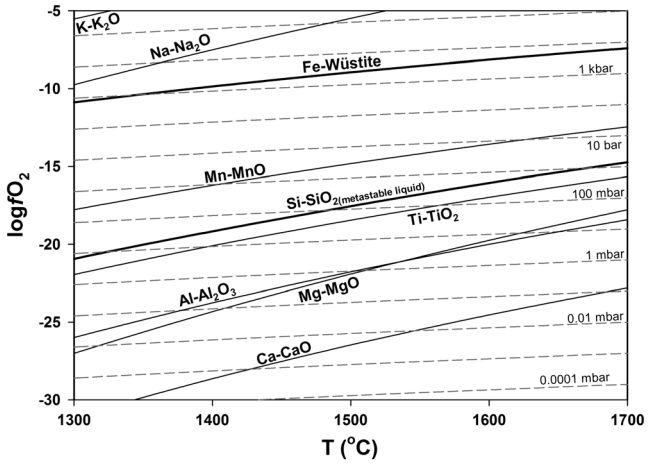

Figure 5. Plot of oxygen fugacity (fO_2) versus temperature (T) over the range of estimated liquidus temperatures of lavas on Mercury. Dashed lines represent the fO_2 of the GCO buffer at specified partial pressures of CO. The solid black lines represent the oxygen fugacities of various metal-metal oxide reactions at 1 bar. The wüstite in the iron-wüstite reaction represents $Fe_{0.947}O$, and the SiO_2 in the Si-SiO_2 reaction represents a metastable SiO_2 melt. Thermodynamic data for all of the calculations obtained from JANAF tables (Chase, 1998).

$$2C_{graphite} + SiO_{2melt} \longleftrightarrow 2CO_{gas} + Si^0{}_{metal} \quad (4)$$

In a system with graphite and silicate melt, the degree to which these reactions proceed to the right depends on the partial pressure of CO (fCO) in equilibrium with graphite, which can be calculated as a function of temperature relative to each of the respective metal oxide reactions. Importantly, the computed CO pressure using the metal oxide reactions represents an upper limit because it assumes the activity of the oxide component in the silicate melt is unity, which is not directly applicable to silicate melts from Mercury.

Figure 5 illustrates the pressure dependence of CO on the fO_2 of the graphite-CO (GCO) buffer relative to the fO_2 of numerous metal-metal oxide reactions as a function of temperature. Based on these calculations and liquidus temperatures for Mercurian lavas of ~1320–1650°C (Namur, Collinet, et al., 2016; Sehlke & Whittington, 2015; Vander Kaaden & McCubbin, 2016), confining pressures in the range of 10 mbar to 1 bar of CO are needed to prevent the formation of Si metal in the presence of graphite, and pressures of about 1 to 8 kbar are needed to prevent the formation of Fe metal (Figure 5). When these pressures are adjusted based on the activities of SiO_2 and FeO in Mercurian magmas (activities were estimated based on the mole fractions of the oxides in each of the nine geochemical terranes from Vander Kaaden et al., 2017), confining pressures in the range of approximately 5 to 700 mbar of CO are needed to prevent the production of Si^0 by smelting, and confining pressures of approximately 10 to 400 bars of CO are needed to prevent the production of Fe^0 by smelting. These pressures indicate that smelting of Fe can occur in the shallow subsurface (up to a maximum depth of approximately 4 km below the surface; Zolotov, 2011) of Mercury during magma ascent, but smelting of Si would be limited to the surfaces of erupted lava flows provided CO pressure could not build overtop erupted lava flows. Given that the lavas are erupting, essentially, into a vacuum on the surface of Mercury (where the surface pressure is on the order of 10^{-14}–10^{-15} bar), buildup of CO pressure over the lava would be a function of several parameters, including (1) kinetics of reactions (1)–(4); (2) kinetics of bubble nucleation, growth, and transport; and (3) the efficiency with which the degassed CO dissipates into the vacuum of the Mercurian surface. Given that there are no obvious obstacles to dissipation, a significant buildup of pressure over a lava flow is unlikely. If dissipation into space is sufficiently rapid, and transport within the magma is likewise rapid, then reaction (4) should have proceeded to the right, resulting in loss of CO and Si smelting. However, the reader is cautioned that a concerted modeling and/or experimental effort would be required to evaluate whether there are regions of parameter space (lava flow thickness, effusion rate, liquidus temperature, and volatile content) for which these suppositions are not valid. Moreover, the kinetics of reactions (1)–(4) relative to the cooling rates of lavas on the surface of Mercury need to be assessed to determine the abundances of metallic phases that could reasonably form as a result of the smelting process. Furthermore, the role of impact melting and remelting processes, which would provide additional time for reactions (1)–(4) to proceed to the right, also need to be built in to any quantitative models for estimating the amount of metallic Si and Fe that could be produced by the smelting process. Nonetheless, smelting likely contributed, at least in part, to the production of Fe and Si metal on Mercury's surface.

Making up the entire O deficit from degassing of CO from reactions (1)–(4) would require that 8.7–11.9 wt % graphite (i.e., 8.7–11.9 wt % of the initial magmas consisted of graphite) was converted to CO through the smelting process. This abundance of graphite implies that as much as 20.2–27.7 wt % CO was degassed from Mercurian lavas. Although this volume of CO is notably high, the presence of a globally extensive, graphite-rich crust on Mercury (Peplowski et al., 2016; Vander Kaaden & McCubbin, 2015a) provides a bountiful source of graphite to facilitate the concomitantly large loss of O. However, Mercury has a low albedo (consistent with the presence of graphite; Murchie et al., 2015) and still has enough O such that 45–71% of the Si is hosted by silicates, implying that reaction (4) did not proceed completely to the right. One possible explanation of this observation is that the net CO dissipation and production yielded pressures of CO over the lava flows in the millibar range (or higher), halting the reaction. However, the apparent incomplete reaction is most easily

explained by the quenching and cooling of lavas at the surface of Mercury outpacing the kinetics of reactions (1)–(4) to produce metal by reaction with graphite, which would freeze the process before it could proceed to completion. Additional support for the latter explanation is provided by the phase equilibria of the evolving chemical system: conversion of SiO_2 to Si metal would increase the Mg/Si ratio of the residual silicate melt (Mg/Si ratio increased by a factor of 1.4–2.2), which in turn, would result in crystallization of mineral phases and possibly quenching of lavas, even if they were to remain at constant temperature. To illustrate this point further, we used the program MAGPOX (Longhi, 1991; Longhi, 1992), adapted for use in MATLAB (Davenport et al., 2014), to compute volatile-free (S and Cl removed) liquidus temperatures for each of the nine geochemical terranes reported by Vander Kaaden et al. (2017), the alkali-free bulk silicate compositions (Table 4), and the alkali-bearing bulk silicate compositions (Table 5). Although MAGPOX has been successfully applied to extraterrestrial compositions in previous studies (Brown & Elkins-Tanton, 2009; Elardo et al., 2015; Goodrich, 1999; Goodrich et al., 2001; Longhi, 1992; Prissel, Parman, & Head, 2016), the compositions in the present study are exotic, so we use the computed liquidus values for purposes of relative comparison only. With the exception of CB and NVP-LMg, the liquidus temperatures of the terrane compositions from the present study are higher than those of the compositions reported by Vander Kaaden et al. (2017) (Tables 4 and 5). This result is consistent with the idea proposed above that the smelting process could result in isothermal quenching of surface lavas. This isothermal-quenching process could help explain why reaction (4) did not go to completion even if CO pressures did not exceed millibar levels. Although the smelting process described herein represents a plausible mechanism to account for at least some of the anomalously low O/Si ratio, additional studies are needed to evaluate the extent to which smelting contributed to the low O/Si ratio on Mercury.

7. Implications of Silicon Smelting on Mercury

7.1. Oxygen Fugacity of the Mercurian Mantle and the Origin of Fe on the Surface

As shown above, the low O/Si ratio on Mercury can be attributed, in part, to a secondary process involving the loss of oxygen from Mercurian lavas through smelting processes on an airless body facilitated by the presence of graphite. The smelting process would also have important implications for estimates of the oxygen fugacity of Mercurian magmas and the origin of S and Fe abundances at the surface. The lower fO_2 estimates (i.e., 5.4 to 7.3 log units below IW; Namur, Charlier, et al., 2016; Namur, Collinet, et al., 2016; Zolotov et al., 2013) are too low to support the 1.0–2.2 wt % FeO calculated for the surface if the Fe is assumed to be Fe^{2+} (McCubbin et al., 2012; Zolotov et al., 2013). Furthermore, the absence of a 1 μm absorption feature in all spectral reflectance data collected from the surface further supports low abundances (≪1.0 wt %) of FeO in silicate minerals (Blewett et al., 1997; Blewett et al., 2013; Ernst et al., 2010; Goudge et al., 2014; Holsclaw et al., 2010; Izenberg et al., 2014; Riner et al., 2010; Vilas, 1988; Weider et al., 2016), leading to speculation that Fe is either hosted in metallic phases or sulfides (Malavergne et al., 2014; Namur, Charlier, et al., 2016; Namur, Collinet, et al., 2016; Namur & Charlier, 2017; Stockstill-Cahill et al., 2012; Vander Kaaden et al., 2017; Vander Kaaden & McCubbin, 2016; Zolotov et al., 2013). Although some groups have advocated that the Fe abundances are reasonable if the Fe is hosted by sulfide phases (Malavergne et al., 2014), the sulfide and iron would both need to be dissolved in the silicate melt to be efficiently transported to the surface through partial melting in the mantle and subsequent volcanism, and under the lower range of fO_2s, Fe solubility in silicate melts is ≪1 wt % Fe (Malavergne et al., 2014; Namur, Charlier, et al., 2016; Vander Kaaden & McCubbin, 2016). Other studies suggested that the Fe may be a metallic phase that was delivered to the surface from an exogenous source; however, the distribution of Fe and its correlation with surface features indicate that Fe is likely indigenous to Mercury (Weider et al., 2014; Weider et al., 2015). Although the elevated S abundances on the surface are explainable by the exceptionally low oxygen fugacity (Malavergne et al., 2014; McCubbin et al., 2012; Namur, Charlier, et al., 2016; Zolotov et al., 2013), the abundances of Fe at the surface remain enigmatic.

The smelting model described in the present study allows for the possibility that Fe was originally dissolved in the silicate melts as FeO and was reduced to Fe^0 during ascent or after eruption. This process would imply that the lower range of magmatic fO_2 on Mercury may be too low for the mantle source region. McCubbin et al. (2012) computed an upper limit on the oxygen fugacity of Mercurian lavas by assuming that all of the Fe was dissolved in parental liquids as Fe^{2+} prior to being transported to the surface. Using the same

methods as McCubbin et al. (2012) and the FeO abundances from the nine geochemical terranes reported by Vander Kaaden et al. (2017), we compute an updated range in fO_2 of 3.2 to 4.3 log units below the IW buffer for the interior of Mercury. Although this fO_2 is toward the oxidizing end of the estimated range of fO_2 for Mercurian magmas, this range in fO_2 is sufficiently reduced to accommodate the measured surface S abundances in silicate liquids (McCubbin et al., 2012; Namur, Charlier, et al., 2016; Vander Kaaden & McCubbin, 2015b), obviating the need for disparate transport mechanisms of Fe and S to the surface. Furthermore, the smelting process would have actively reduced the surface lavas resulting in the formation of Fe metal and/or Fe sulfides and preventing Fe^{2+} from entering silicate minerals, which satisfies the constraints from spectral reflectance observations. Although, Fe^{2+} may have been incorporated into minerals that crystallized at depths near or below the initiation of smelting.

The Si-smelting process would indicate that the surface is within approximately a log unit of the Si-SiO_2 buffer, which is about 8.7 to 12.1 log units below the IW buffer over the range of estimated liquidus temperatures for Mercurian lavas of 1360–1650°C (Namur, Collinet, et al., 2016; Sehlke & Whittington, 2015). The surface estimates for fO_2 in the present study are several log units more reduced than the lower estimates for Mercury fO_2 in previous studies (McCubbin et al., 2012; Namur, Charlier, et al., 2016; Namur, Collinet, et al., 2016; Zolotov et al., 2013). If the smelting process described in the present study has occurred at the surface, it implies that Mercury is further distinguished from other terrestrial planets, which typically have interiors that are more reduced than their surfaces (e.g., Sharp et al., 2013; Trail et al., 2011).

7.2. Magmatic Degassing in Mercurian Lavas and Implications for Explosive Volcanism

There exists a preponderance of geomorphic evidence for explosive volcanism on Mercury (Besse et al., 2015; Head et al., 2008; Head et al., 2009; Kerber et al., 2011; Kerber et al., 2009; Prockter et al., 2010; Thomas et al., 2014a; Thomas et al., 2014b; Thomas et al., 2015), and there has been some effort to identify the vapor species responsible for assisting these eruptions (Kerber et al., 2009; Weider et al., 2016; Zolotov, 2011; Zolotov et al., 2013). Given that numerous vapor species occur as a byproduct of smelting reactions (1)–(4), we consider the implications for smelting on the production of gas species and whether or not they could play a role in explosive volcanism on Mercury.

Even if Si-smelting (reaction (4)) were the primary process that led to the observed O/Si ratio, it could not account for explosive volcanism because reaction (4) requires low pressures of CO, in the range of 10–1000 mbar (Figure 5), to facilitate Si reduction. Therefore, much of the CO production from reaction (4) must occur on the surface, subsequent to eruption. In contrast, reaction (1) will proceed at higher pressures, in the range of 10 to 400 bars. Consequently, if graphite is entrained in the lavas at depth, they could begin to produce CO vapor at depths as great as 4 km below the surface. In fact, the range in Fe abundances of the nine geochemical terranes implies that 0.38–0.85 wt % CO could have been produced at depth during ascent if all the FeO was reduced by graphite to Fe^0. This mass of CO would translate to an even greater volume fraction of CO that would have contributed substantially to explosive volcanic processes on Mercury in a process very similar to that proposed for graphite-induced explosive volcanism on the Moon (Fogel & Rutherford, 1995; Head & Wilson, 2017; Nicholis & Rutherford, 2009; Rutherford & Papale, 2009; Sato, 1979; Wilson & Head, 2017). In fact, graphite oxidation has been proposed previously as a mechanism for explosive volcanism on Mercury (Weider et al., 2016; Zolotov, 2011). In particular, a pyroclastic deposit northeast of the Rachmaninoff basin is depleted in C, exhibits high overall reflectance, and exhibits a spectral absorption feature consistent with 0.03–0.1 wt % FeO (Weider et al., 2016). This particular deposit could represent a case where the abundance of graphite was insufficient to reduce all of the Fe, leaving some FeO to be incorporated into silicate phases. Alternatively, Weider et al. (2016) have suggested that the oxygen-metal charge transfer band in VIRS spectra are saturated in most terranes and supportive of FeO abundances of up to several tenths of a wt % across the surface (Goudge et al., 2014; Weider et al., 2016), which would be consistent with the presence of minor amounts of mineral phases in erupted lavas that crystallized at depth prior to the initiation of smelting.

Reactions (2) and (3) have both CO vapor and alkali metal vapor as products of the smelting reaction. Furthermore, it appears from Figure 5 that substantial pressures of CO are required to prevent reduction of Na and K oxide components to metal, which initially implies that these reactions could contribute (substantially in the case of Na) to explosive volcanic processes on Mercury. However, there is not sufficient

experimental data on the stability of alkali metal vapors as a function of pressure in systems relevant to Mercury, and the limited data that are available suggest that the alkalis retain their lithophile character at pressure (Namur, Collinet, et al., 2016; Vander Kaaden & McCubbin, 2016). Consequently, we are unable to determine the degree to which reactions (2) and (3) contributed to explosive volcanic processes on Mercury; however, we note that this topic could be a fruitful avenue of future research.

In addition to the vapor species that would be involved in the smelting process, there are a number of additional vapor species that could have or have been purported to assist explosive volcanic processes on Mercury. The role of sulfur in volcanic degassing is important to consider given the elevated abundances of S on the surface of Mercury and the fact that SO_2 is a dominant product of volcanic emissions on Earth (Allard et al., 1994; Halmer et al., 2002; Oppenheimer et al., 2014; Scaillet et al., 1998; Self et al., 2006). However, with the exception of H_2S, many of the volcanic emissions of sulfur are related to oxidized sulfur species (Behrens & Gaillard, 2006; Metrich & Mandeville, 2010; Scaillet et al., 1998), which should occur in miniscule abundances at oxygen fugacities relevant to Mercury's surface (Bell et al., 2015; Metrich & Mandeville, 2010; Scaillet et al., 1998; Zolotov, 2011; Zolotov et al., 2013). Furthermore, many of the sulfide phases expected to occur on Mercury are highly refractory (e.g., CaS and MgS both have melting temperatures in excess of 2000°C; Anthony et al., 2001; Lide, 2000), and they would not be amenable to forming a sulfide vapor phase. Nonetheless, there is evidence that S has played a role in explosive volcanic processes on Mercury because the same pyroclastic deposit northeast of the Rachmaninoff basin that is depleted in C is also depleted in S relative to the rest of the surface (Weider et al., 2016). The implication of S degassing playing a role in explosive volcanic processes on Mercury also implicates a role for H given that H_2S and mixed Cl-O-H-S vapors are among the only reduced sulfide vapor species that would be stable under Mercurian conditions (Bell et al., 2015; Scaillet et al., 1998). Furthermore, if H_2S was present, it would imply that some H_2 may also occur, which is the dominant form of H in the O-H system under Mercurian conditions. Of the other magmatic volatiles to consider, Cl has been measured as a minor component on the Mercurian surface. Based on the oxygen fugacity of Mercurian magmas and lavas, Cl could have been a minor contributor to volcanic emissions in the form of alkali-chlorides (Evans et al., 2015; Zolotov, 2011), HCl, Cl, or Cl-S vapors (Bell et al., 2015; Fegley & Zolotov, 2000).

In summary, the smelting processes hypothesized in the present study to account, in part, for the low O/Si ratio would produce volatile species that can contribute to explosive volcanism on Mercury. The primary vapor constituent that would facilitate these explosive eruptions is CO, with contributions from other vapors in the Cl-O-H-S system. Additionally, alkali metals could have also contributed to the vapor phase, but additional work is needed to assess the importance of their roles.

7.3. Implications for the Chemistry and Mineralogy of Mercury's Mantle

The low O/Si weight ratio of 1.2 ± 0.1 reported in the present study is best explained by the loss of oxygen from the regolith by space weathering and from Mercurian lavas through smelting of Fe, Si, and possibly alkalis (i.e., Na and K) facilitated by the presence of graphite that was entrained in the ascending magmas and erupted lavas. Numerous studies have used MESSENGER data to understand the thermochemical evolution of Mercury, but all of the studies were published prior to the realization that the O/Si ratio is exceptionally low. Therefore, it is important to assess the implications of the low O/Si ratio on the previous studies and interpretations of Mercury's interior.

The loss of oxygen by a secondary process, as favored in the present study to account for the low O/Si ratio, primarily results in the loss of CO and possibly mobilization of alkalis. Consequently, the ratios of elements (i.e., Ti, Al, Cr, Fe, Mn, Mg, Ca, S, and Cl) to Si, which were used to derive the terrane compositions and experimental starting compositions in previous studies, should not have changed during either of the proposed O-loss processes because the systems would have remained closed with respect to these ratios if only CO was lost. Although the alkali abundances could have been affected by these processes given their volatile nature at low pressure and high temperature, the abundances of alkalis across the planet are averaged into two latitudinal bins (Peplowski et al., 2011; Peplowski et al., 2014), so there was already poor resolution on the alkali abundances in each of the geochemical terranes (Vander Kaaden et al., 2017; Weider et al., 2015). Consequently, if secondary O-loss processes are indeed responsible for the low O/Si ratio on Mercury, it implies that the assumed valences of the elements measured by MESSENGER (i.e., Si^{4+}, Ti^{4+}, Al^{3+}, $Cr^{2+/3+}$, Fe^{2+}, Mn^{2+}, Mg^{2+}, Ca^{2+}, Na^{+}, K^{+}, S^{2-}, and Cl^{-}) were relevant to the compositions of boninitic and

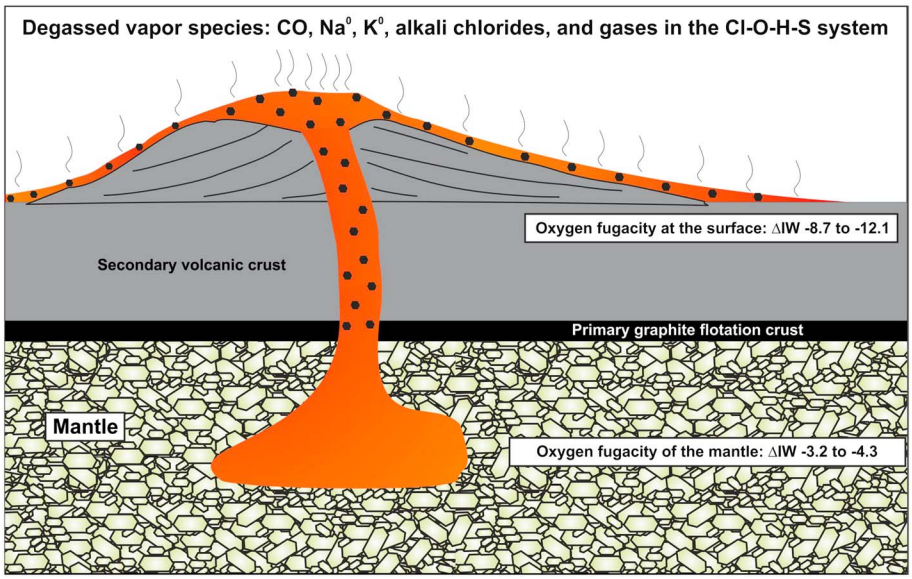

Figure 6. Cartoon illustrating the smelting and concomitant degassing model presented in the present study to account for the low O/Si ratio measured on Mercury. The model shows the stages of partial melting, magma ascent and entrainment of graphite, eruption, and degassing. The mantle as well as the primary and secondary crust are indicated, and we have depicted the computed values for the oxygen fugacity of the mantle source and the surface. Additionally, we show that graphite is entrained in magmas both during ascent and as the lavas flow across the surface. We have also indicated the vapor species at the volcanic vent and those over the lava flow. Finally, we indicated the various zones over which the Fe, Na, K, and Si will be reduced.

komatiitic parental liquids that formed through partial melting processes in the Mercurian mantle (Namur, Collinet, et al., 2016; Nittler et al., 2011; Stockstill-Cahill et al., 2012; Vander Kaaden & McCubbin, 2016; Vander Kaaden et al., 2017). Furthermore, the interpretations regarding the thermochemical evolution of Mercury's interior and mantle mineralogy reported in previous studies were, fortuitously, unaffected by the fact that the low O/Si ratio of the surface was not considered (e.g., Charlier et al., 2013; Namur, Charlier, et al., 2016; Namur, Collinet, et al., 2016; Namur & Charlier, 2017; Nittler et al., 2011; Stockstill-Cahill et al., 2012; Vander Kaaden & McCubbin, 2015a; Vander Kaaden & McCubbin, 2016; Vander Kaaden et al., 2017; Weider et al., 2014; Weider et al., 2015). The assumptions made in the previous studies about the valences of cations were relevant to the pre-smelting and pre–space weathering compositions that they were intended to represent, and hence, they yielded useful information about the interior of Mercury. However, previous studies of the mineralogy of the present-day surface likely need to be substantially revised based on the results reported in the present study through additional experimental campaigns.

8. Summary

The surface of Mercury has an anomalously low O/Si weight ratio of 1.2 ± 0.1 (Figure 1), which was determined by analysis of GRS data from the MESSENGER spacecraft. The low O/Si ratio indicates that surface materials are composed of 12–20% metallic phases that consist largely of Si-rich, Si-Fe alloys. The low O/Si ratio is not a primary feature of the silicate portion of Mercury and is likely the result of secondary processes involving the loss of oxygen by a combination of space weathering and graphite-induced smelting of Si and Fe from silicate melts. The smelting processes described herein is depicted by the cartoon in Figure 6. This model indicates that partial melting took place in the Mercurian mantle under a modestly low oxygen fugacity of 3.2 to 4.3 log units below the IW buffer. These partial melts ascended through the mantle and came into contact with the graphite-rich crust. Graphite was then entrained in the magmas as they continued their ascent. Once the confining pressure was less than 400 bars, FeO (and possibly Na_2O and K_2O) reduced to metals, producing a substantial volume of CO that helped to facilitate eruption, possibly aided by reduced H and S species. Once the lavas erupted and flowed across the surface, additional graphite was entrained in the lavas from the surface materials. The confining pressure over the lava flows at the surface would have been

low, given the efficiency with which degassing vapor would dissipate into a 10^{-14}–10^{-15} bar atmosphere. In fact, this low confining pressure would facilitate the reduction of SiO_2 melt components to Si metal as long as there was less than about 10 mbar of confining pressure of CO over the lava flows. As SiO_2 was reduced to Si^0, it would have raised the Mg/Si ratio of the residual melt, promoting crystallization. The lavas would then quench, and space weathering processes would further work toward reduction of Fe and Si components of surface materials, aided by the presence of graphite. Impact melting processes and regolith gardening would initiate further cycles of the same two processes until we produced the present day surface materials with a low O/Si ratio, which are comprised of silicates, oxides, sulfides, and Fe-Si alloys.

Acknowledgments
We thank Donald Lindsley for insightful discussions regarding the stability of alkali metal vapors under reducing conditions. We thank Justin Filiberto for the editorial handling of the manuscript, and we thank insightful and constructive reviews from Mikhail Zolotov and Stephen Parman that improved the quality of the manuscript. This work was supported by NASA through the Solar System Workings Program grants awarded to F. M.M. and S. M. E. (NNX16AQ17G) and through the Discovery Program contract NAS5-97271 to the Johns Hopkins University Applied Physics Laboratory and NASW-00002 to the Carnegie Institution of Washington. MESSENGER data are available through the NASA Planetary Data System.

References

Allard, P., Carbonnelle, J., Metrich, N., Loyer, H., & Zettwoog, P. (1994). Sulfur output and magma degassing budget of Stromboli Volcano. *Nature*, *368*(6469), 326–330.

Anand, M., Taylor, L. A., Nazarov, M. A., Shu, J., Mao, H. K., & Hemley, R. J. (2004). Space weathering on airless planetary bodies: Clues from the lunar mineral hapkeite. *Proceedings of the National Academy of Sciences of the United States of America*, *101*(18), 6847–6851.

Anthony, J. W., Bideaux, R. A., Bladh, K. W., & Nichols, M. C. (2001). *Handbook of mineralogy, 1* (pp. 588). Chantilly, VA: Mineralogical Society of America.

Aoudjehane, H. C., Avice, G., Barrat, J. A., Boudouma, O., Chen, G., Duke, M. J., … Zanda, B. (2012). Tissint Martian meteorite: A fresh look at the interior, surface, and atmosphere of Mars. *Science*, *338*(6108), 785–788.

Bafghi, M. S., Fukuda, M., Ito, Y., Yamada, S., & Sano, M. (1993). Effect of CO gas formation on reduction rate of iron oxide in molten slag by graphite. *ISIJ International*, *33*(11), 1125–1130.

Bafghi, M. S., Kurimoto, H., & Sano, M. (1992). Effect of slag foaming on the reduction of iron oxide in molten slag by graphite. *ISIJ International*, *32*(10), 1084–1090.

Behrens, H., & Gaillard, F. (2006). Geochemical aspects of melts: Volatiles and redox behavior. *Elements*, *2*(5), 275–280.

Bell, A. S., Shearer, C., deMoor, J. M., & Provencio, P. (2015). Using the sulfide replacement petrology in lunar breccia 67915 to construct a thermodynamic model of S-bearing fluid in the lunar crust. *Geochimica et Cosmochimica Acta*, *171*, 50–60.

Besse, S., Doressoundiram, A., & Benkhoff, J. (2015). Spectroscopic properties of explosive volcanism within the Caloris basin with MESSENGER observations. *Journal of Geophysical Research: Planets*, *120*, 2102–2117. https://doi.org/10.1002/2015JE004819

Bird, J. M., & Weathers, M. S. (1977). Native iron occurences of Disko Island, Greenland. *Journal of Geology*, *85*(3), 359–371.

Blewett, D. T., Lucey, P. G., Hawke, B. R., Ling, G. G., & Robinson, M. S. (1997). A comparison of Mercurian reflectance and spectral quantities with those of the Moon. *Icarus*, *129*(1), 217–231.

Blewett, D. T., Stadermann, A. C., Susorney, H. C., Ernst, C. M., Xiao, Z., Chabot, N. L., … Solomon, S. C. (2016). Analysis of MESSENGER high-resolution images of Mercury's hollows and implications for hollow formation. *Journal of Geophysical Research: Planets*, *121*, 1798–1813. https://doi.org/10.1002/2016JE005070

Blewett, D. T., Vaughan, W. M., Xiao, Z., Chabot, N. L., Denevi, B. W., Ernst, C. M., … Solomon, S. C. (2013). Mercury's hollows: Constraints on formation and composition from analysis of geological setting and spectral reflectance. *Journal of Geophysical Research: Planets*, *118*, 1013–1032. https://doi.org/10.1029/2012JE004174

Borin, P., Cremonese, G., Marzari, F., Bruno, M., & Marchi, S. (2009). Statistical analysis of micrometeoroids flux on Mercury. *Astronomy & Astrophysics*, *503*(1), 259–264.

Brown, S. M., & Elkins-Tanton, L. T. (2009). Compositions of Mercury's earliest crust from magma ocean models. *Earth and Planetary Science Letters*, *286*(3–4), 446–455.

Burnham, C. W. (1994). Development of the Burnham model for prediction of H_2O solubility in magmas. In M. R. Carroll & J. R. Holloway (Eds.), *Volatiles in Magmas. Reviews in Mineralogy* (Vol. 30, pp. 123–129). Washington, DC: Mineral Society of America.

Byrne, P. K., Ostrach, L. R., Fassett, C. I., Chapman, C. R., Denevi, B. W., Evans, A. J., … Solomon, S. C. (2016). Widespread effusive volcanism on Mercury likely ended by about 3.5Ga. *Geophysical Research Letters*, *43*, 7408–7416. https://doi.org/10.1002/2016GL069412

Carroll, M. R., & Webster, J. D. (1994). Solubilities of sulfur, noble-gases, nitrogen, chlorine, and fluorine in magmas. In M. R. Carroll, & J. R. Holloway (Eds.), *Volatiles in Magmas. Reviews in Mineralogy* (Vol. 30, pp. 231–279). Washington, DC: Mineralogical Society of America.

Charlier, B., Grove, T. L., & Zuber, M. T. (2013). Phase equilibria of ultramafic compositions on Mercury and the origin of the compositional dichotomy. *Earth and Planetary Science Letters*, *363*, 50–60.

Chase, M. W. (1998). NIST-JANAF thermochemical tables. In *Journal of Physical and Chemical Reference Data, 9* (1961 pp.). Gaithersburg, MD: National Institute of Standards and Technology.

Cintala, M. J. (1992). Impact-induced thermal effects in the lunar and Mercurian regoliths. *Journal of Geophysical Research*, *97*(E1), 947–973. https://doi.org/10.1029/91JE02207

Cross, W., Iddings, J. P., Pirsson, L. V., & Washington, H. (1903). *Quantitative classification of igneous rocks*. Chicago, IL: University of Chicago Press.

Dasgupta, R., & Hirschmann, M. M. (2010). The deep carbon cycle and melting in Earth's interior. *Earth and Planetary Science Letters*, *298*(1-2), 1–13.

Davenport, J. D., Longhi, J., Neal, C. R., Jolliff, B. L., & Bolster, B. J., (2014). Simulating planetary igneous crystallization environments (SPICEs): A suite of igneous crystallization programs. Presented at the Proceedings of the 45th Lunar and Planetary Science Conference (1111 pp.). Woodlands, TX: Lunar and Planetary Institute.

Dixon, J. E., & Stolper, E. M. (1995). An experimental study of water and carbon dioxide solubilities in mid-ocean ridge basaltic liquids: 2. Applications to degassing. *Journal of Petrology*, *36*, 1633–1646.

Dixon, J. E., Stolper, E. M., & Holloway, J. R. (1995). An experimental study of water and carbon dioxide solubilities in mid ocean ridge basaltic liquids .1. Calibration and solubility models. *Journal of Petrology*, *36*, 1607–1631.

Domingue, D. L., Chapman, C. R., Killen, R. M., Zurbuchen, T. H., Gilbert, J. A., Sarantos, M., … McClintock, W. E. (2014). Mercury's weather-beaten surface: Understanding Mercury in the context of lunar and asteroidal space weathering studies. *Space Science Reviews*, *181*(1-4), 121–214.

Eggler, D. H., Mysen, B. O., Hoering, T. C., & Holloway, J. R. (1979). Solubility of carbon monoxide in silicate melts at high pressure and its effect on silicate phase relations. *Earth and Planetary Science Letters*, *43*(2), 321–330.

Ehlmann, B. L., Anderson, F. S., Andrews-Hanna, J., Catling, D. C., Christensen, P. R., Cohen, B. A., … Zahnle, K. J. (2016). The sustainability of habitability on terrestrial planets: Insights, questions, and needed measurements from Mars for understanding the evolution of Earth-like worlds. *Journal of Geophysical Research: Planets*, *121*, 1927–1961. https://doi.org/10.1002/2016JE005134

Ehrlich, P. (1963). Alkaline earth metals. In G. Brauer (Ed.), *Handbook of preparative inorganic chemistry* (pp. 887–949). New York, NY: Academic Press.

Elardo, S. M., Shearer, C. K., Kaaden, K. E. V., McCubbin, F. M., & Bell, A. S. (2015). Petrogenesis of primitive and evolved basalts in a cooling Moon: Experimental constraints from the youngest known lunar magmas. *Earth and Planetary Science Letters*, *422*, 126–137.

Ernst, C. M., Murchie, S. L., Barnouin, O. S., Robinson, M. S., Denevi, B. W., Blewett, D. T., … Roberts, J. H. (2010). Exposure of spectrally distinct material by impact craters on Mercury: Implications for global stratigraphy. *Icarus*, *209*(1), 210–223.

Evans, L. G., Peplowski, P. N., McCubbin, F. M., McCoy, T. J., Nittler, L. R., Zolotov, M. Y., … Solomon, S. C. (2015). Chlorine on the surface of Mercury: MESSENGER gamma-ray measurements and implications for the planet's formation and evolution. *Icarus*, *257*, 417–427.

Evans, L. G., Peplowski, P. N., Rhodes, E. A., Lawrence, D. J., McCoy, T. J., Nittler, L. R., … Goldsten, J. O. (2012). Major-element abundances on the surface of Mercury: Results from the MESSENGER Gamma-Ray Spectrometer. *Journal of Geophysical Research*, *117*, E00L07. https://doi.org/10.1029/2012JE004178

Fegley, B., & Zolotov, M. Y. (2000). Chemistry of sodium, potassium, and chlorine in volcanic gases on Io. *Icarus*, *148*(1), 193–210.

Fogel, R. A., & Rutherford, M. J. (1995). Magmatic volatiles in primitive lunar glasses part 1: FTIR and EPMA analyses of Apollo 15 green and yellow glasses and revision of the volatile-assisted fire-fountain theory. *Geochimica et Cosmochimica Acta*, *59*(1), 201–215.

Goodrich, C. A. (1999). Are ureilites residues from partial melting of chondritic material? The answer from MAGPOX. *Meteoritics & Planetary Science*, *34*(1), 109–119.

Goodrich, C. A., Fioretti, A. M., Tribaudino, M., & Molin, G. (2001). Primary trapped melt inclusions in olivine in the olivine-augite-orthopyroxene ureilite Hughes 009. *Geochimica et Cosmochimica Acta*, *65*(4), 621–652.

Goodrich, C. A., Van Orman, J. A., & Wilson, L. (2007). Fractional melting and smelting on the ureilite parent body. *Geochimica et Cosmochimica Acta*, *71*(11), 2876–2895.

Gopon, P., Spicuzza, M. J., Kelly, T. F., Reinhard, D., Prosa, T. J., & Fournelle, J. (2017). Ultra-reduced phases in Apollo 16 regolith: Combined field emission electron probe microanalysis and atom probe tomography of submicron Fe-Si grains in Apollo 16 sample 61500. *Meteoritics & Planetary Science*, *52*(9), 1941–1962.

Goudge, T. A., Head, J. W., Kerber, L., Blewett, D. T., Denevi, B. W., Domingue, D. L., … Solomon, S. C. (2014). Global inventory and characterization of pyroclastic deposits on Mercury: New insights into pyroclastic activity from MESSENGER orbital data. *Journal of Geophysical Research: Planets*, *119*, 635–658. https://doi.org/10.1002/2013JE004480

Halmer, M. M., Schmincke, H. U., & Graf, H. F. (2002). The annual volcanic gas input into the atmosphere, in particular into the stratosphere: a global data set for the past 100 years. *Journal of Volcanology and Geothermal Research*, *115*, 511–528.

Hansen, M. (1958). *Constitution of binary alloys*. *Metallurgy and Metallurgical Engineering Series* (pp. 1305). New York: McGraw-Hill Book Company.

Hapke, B. (2001). Space weathering from Mercury to the asteroid belt. *Journal of Geophysical Research*, *106*(E5), 10039–10073. https://doi.org/10.1029/2000JE001338

Head, J. W., Murchie, S. L., Prockter, L. M., Robinson, M. S., Solomon, S. C., Strom, R. G., … Gillis-Davis, J. J. (2008). Volcanism on Mercury: Evidence from the first MESSENGER flyby. *Science*, *321*(5885), 69–72.

Head, J. W., Murchie, S. L., Prockter, L. M., Solomon, S. C., Chapman, C. R., Strom, R. G., … Kerber, L. (2009). Volcanism on Mercury: Evidence from the first MESSENGER flyby for extrusive and explosive activity and the volcanic origin of plains. *Earth and Planetary Science Letters*, *285*, 227–242.

Head, J. W., & Wilson, L. (2017). Generation, ascent and eruption of magma on the Moon: New insights into source depths, magma supply, intrusions and effusive/explosive eruptions (Part 2: Predicted emplacement processes and observations). *Icarus*, *283*, 176–223.

Hentzell, H. T. G., Robertsson, A., Hultman, L., Shaofang, G., Hörnström, S.-E., & Psaras, P. A. (1987). Formation of aluminum silicide between two layers of amorphous silicon. *Applied Physics Letters*, *50*, 933–934.

Hirschmann, M. M., & Withers, A. C. (2008). Ventilation of CO_2 from a reduced mantle and consequences for the early martian greenhouse. *Earth and Planetary Science Letters*, *270*(1–2), 147–155.

Hirschmann, M. M., Withers, A. C., Ardia, P., & Foley, N. T. (2012). Solubility of molecular hydrogen in silicate melts and consequences for volatile evolution of terrestrial planets. *Earth and Planetary Science Letters*, *345*, 38–48.

Holloway, J. R., & Jakobsson, S. (1986). Volatile solubilities in magmas: Transport of volatiles from mantles to planet surfaces. *Journal of Geophysical Research*, *91*, D505–D508. https://doi.org/10.1029/JB091iB04p0D505

Holsclaw, G. M., McClintock, W. E., Domingue, D. L., Izenberg, N. R., Blewett, D. T., & Sprague, A. L. (2010). A comparison of the ultraviolet to near-infrared spectral properties of Mercury and the Moon as observed by MESSENGER. *Icarus*, *209*(1), 179–194.

Iacono-Marziano, G., Gaillard, F., Scaillet, B., Polozov, A. G., Marecal, V., Pirre, M., & Arndt, N. T. (2012). Extremely reducing conditions reached during basaltic intrusion in organic matter-bearing sediments. *Earth and Planetary Science Letters*, *357*, 319–326.

Izenberg, N. R., Klima, R. L., Murchie, S. L., Blewett, D. T., Holsclaw, G. M., McClintock, W. E., … Dyar, M. D. (2014). The low-iron, reduced surface of Mercury as seen in spectral reflectance by MESSENGER. *Icarus*, *228*, 364–374.

Jambon, A. (1994). Earth degassing and large-scale geochemical cycling of volatile elements. *Volatiles in Magmas*, *30*, 479–517.

Keller, L. P., & McKay, D. S. (1993). Discovery of vapor deposits in the lunar regolith. *Science*, *261*(5126), 1305–1307.

Keller, L. P., & McKay, D. S. (1997). The nature and origin of rims on lunar soil grains. *Geochimica et Cosmochimica Acta*, *61*(11), 2331–2341.

Kerber, L., Head, J. W., Blewett, D. T., Solomon, S. C., Wilson, L., Murchie, S. L., … Domingue, D. L. (2011). The global distribution of pyroclastic deposits on Mercury: The view from MESSENGER flybys 1-3. *Planetary and Space Science*, *59*(15), 1895–1909.

Kerber, L., Head, J. W., Solomon, S. C., Murchie, S. L., Blewett, D. T., & Wilson, L. (2009). Explosive volcanic eruptions on Mercury: Eruption conditions, magma volatile content, and implications for interior volatile abundances. *Earth and Planetary Science Letters*, *285*(3-4), 263–271.

Lawrence, D. J., Peplowski, P. N., Beck, A. W., Feldman, W. C., Frank, E. A., McCoy, T. J., … Solomon, S. C. (2017). Compositional terranes on Mercury: Information from fast neutrons. *Icarus*, *281*, 32–45.

Lehnert, K., Su, Y., Langmuir, C. H., Sarbas, B., & Nohl, U. (2000). A global geochemical database structure for rocks. *Geochemistry, Geophysics, Geosystems*, *1*(5), 1012. https://doi.org/10.1029/1999GC000026

Li, Y., Dasgupta, R., & Tsuno, K. (2017). Carbon contents in reduced basalts at graphite saturation: Implications for the degassing of Mars, Mercury, and the Moon. *Journal of Geophysical Research: Planets*, *122*, 1300–1320. https://doi.org/10.1002/2017JE005289

Lide, D. R. (2000). *CRC handbook of chemistry and physics, 2000–2001 : A ready-reference book of chemical and physical data*. Boca Raton, FL: CRC Press.
Lodders, K. (2003). Solar system abundances and condensation temperatures of the elements. *Astrophysical Journal*, *591*(2), 1220–1247.
Lodders, K., & Fegley, B. (1998). *The planetary scientist's companion*. New York: Oxford University Press.
Longhi, J. (1991). Comparative liquidus equilibria of hypersthene-normative basalts at low pressure. *American Mineralogist*, *76*, 785–800.
Longhi, J. (1992). Origin of picritic green glass magmas by polybaric fractional fusion. *Proceedings of Lunar and Planetary Science*, *22*, 343–353.
Lucey, P. G., & Noble, S. K. (2008). Experimental test of a radiative transfer model of the optical effects of space weathering. *Icarus*, *197*(1), 348–353.
Lucey, P. G., & Riner, M. A. (2011). The optical effects of small iron particles that darken but do not redden: Evidence of intense space weathering on Mercury. *Icarus*, *212*(2), 451–462.
Malavergne, V., Cordier, P., Righter, K., Brunet, F., Zanda, B., Addad, A., … Hewins, R. H. (2014). How Mercury can be the most reduced terrestrial planet and still store iron in its mantle. *Earth and Planetary Science Letters*, *394*, 186–197.
Marchi, S., Chapman, C. R., Fassett, C. I., Head, J. W., Bottke, W. F., & Strom, R. G. (2013). Global resurfacing of Mercury 4.0-4.1 billion years ago by heavy bombardment and volcanism. *Nature*, *499*(7456), 59–61.
Marchi, S., Mottola, S., Cremonese, G., Massironi, M., & Martellato, E. (2009). A new chronology for the Moon and Mercury. *Astronomical Journal*, *137*(6), 4936–4948.
McCubbin, F. M., Riner, M. A., Vander Kaaden, K. E., & Burkemper, L. K. (2012). Is Mercury a volatile-rich planet? *Geophysical Research Letters*, *39*, L09202. https://doi.org/10.1029/2012GL051711
Melson, W. G., & Switzer, G. (1966). Plagioclase-spinel-graphite xenoliths in metallic iron-bearing basalts, Disko Island, Greenland. *American Mineralogist*, *51*, 664–676.
Metrich, N., & Mandeville, C. W. (2010). Sulfur in magmas. *Elements*, *6*(2), 81–86.
Miller, P. D., Lee, J. G., & Cutler, I. B. (1979). Reduction of silica with carbon and silicon carbide. *Journal of the American Ceramic Society*, *62*(3-4), 147–149.
Morris, R. V. (1980). *Origins and size distribution of metallic iron particles in the lunar regolith*. *Proceedings of the 11th Lunar and Planetary science Conference* (pp. 1697–1712). New York: Pergamon Press.
Murchie, S. L., Klima, R. L., Denevi, B. W., Ernst, C. M., Keller, M. R., Domingue, D. L., … Solomon, S. C. (2015). Orbital multispectral mapping of Mercury with the MESSENGER Mercury Dual Imaging System: Evidence for the origins of plains units and low-reflectance material. *Icarus*, *254*, 287–305.
Mysen, B. O., Fogel, M. L., Morrill, P. L., & Cody, G. D. (2009). Solution behavior of reduced C-O-H volatiles in silicate melts at high pressure and temperature. *Geochimica et Cosmochimica Acta*, *73*(6), 1696–1710.
Namur, O., & Charlier, B. (2017). Silicate mineralogy at the surface of Mercury. *Nature Geoscience*, *10*, 9–13.
Namur, O., Charlier, B., Holtz, F., Cartier, C., & McCammon, C. (2016). Sulfur solubility in reduced mafic silicate melts: Implications for the speciation and distribution of sulfur on Mercury. *Earth and Planetary Science Letters*, *448*, 102–114.
Namur, O., Collinet, M., Charlier, B., Grove, T. L., Holtz, F., & McCammon, C. (2016). Melting processes and mantle sources of lavas on Mercury. *Earth and Planetary Science Letters*, *439*, 117–128.
Nelson, R. O., Chadwick, M. B., Michaudon, A., & Young, P. G. (2001). High-resolution measurements and calculations of photon-production cross sections for O-16($n,x\gamma$) reactions induced by neutrons with energies between 4 and 200 MeV. *Nuclear Science and Engineering*, *138*(2), 105–144.
Newcombe, M. E., Brett, A., Beckett, J. R., Baker, M. B., Newman, S., Guan, Y., … Stolper, E. M. (2017). Solubility of water in lunar basalt at low pH_2O. *Geochimica et Cosmochimica Acta*, *200*, 330–352.
Nicholis, M. G., & Rutherford, M. J. (2009). Graphite oxidation in the Apollo 17 orange glass magma: Implications for the generation of a lunar volcanic gas phase. *Geochimica et Cosmochimica Acta*, *73*(19), 5905–5917.
Nittler, L. R., McCoy, T. J., Clark, P. E., Murphy, M. E., Trombka, J. I., & Jarosewich, E. (2004). Bulk element compositions of meteorites: A guide for interpreting remote-sensing geochemical measurements of planets and asteroids. *Antarctic Meteorite Research*, *17*, 233–253.
Nittler, L. R., Starr, R. D., Weider, S. Z., McCoy, T. J., Boynton, W. V., Ebel, D. S., … Sprague, A. L. (2011). The major-element composition of Mercury's surface from MESSENGER X-ray spectrometry. *Science*, *333*(6051), 1847–1850.
Noble, S. K., Keller, L. P., & Pieters, C. M. (2005). Evidence of space weathering in regolith breccias I: Lunar regolith breccias. *Meteoritics & Planetary Science*, *40*(3), 397–408.
Noble, S. K., & Pieters, C. M. (2003). Space weathering on Mercury: Implications for remote sensing. *Solar System Research*, *37*(1), 31–35.
Noble, S. K., Pieters, C. M., & Keller, L. P. (2007). An experimental approach to understanding the optical effects of space weathering. *Icarus*, *192*(2), 629–642.
Noble, S. K., Pieters, C. M., Taylor, L. A., Morris, R. V., Allen, C. C., McKay, D. S., & Keller, L. P. (2001). The optical properties of the finest fraction of lunar soil: implications for space weathering. *Meteoritics & Planetary Science*, *36*(1), 31–42.
Noguchi, T., Kimura, M., Hashimoto, T., Konno, M., Nakamura, T., Zolensky, M. E., … Ishibashi, Y. (2014a). Space weathered rims found on the surfaces of the Itokawa dust particles. *Meteoritics & Planetary Science*, *49*(2), 188–214.
Noguchi, T., Kimura, M., Hashimoto, T., Konno, M., Nakamura, T., Zolensky, M. E., … Okada, T. (2014b). Sylvite and halite on particles recovered from 25143 Itokawa: A preliminary report. *Meteoritics & Planetary Science*, *49*(7), 1305–1314.
Noguchi, T., Nakamura, T., Kimura, M., Zolensky, M. E., Tanaka, M., Hashimoto, T., … Okazaki, R. (2011). Incipient space weathering observed on the surface of Itokawa dust particles. *Science*, *333*(6046), 1121–1125.
O'Neill, H. S. C., & Eggins, S. M. (2002). The effect of melt composition on trace element partitioning: An experimental investigation of the activity coefficients of FeO, NiO, CoO, MoO_2 and MoO_3 in silicate melts. *Chemical Geology*, *186*(1-2), 151–181.
Oppenheimer, C., Fischer, T. P., & Scaillet, B. (2014). Volcanic degassing: Process and impact A2 - Holland, Heinrich D. In K. K. Turekian (Ed.), *Treatise on geochemistry* (2nd ed., pp. 111–179). Oxford: Elsevier.
Peplowski, P. N., Bazell, D., Evans, L. G., Goldsten, J. O., Lawrence, D. J., & Nittler, L. R. (2015). Hydrogen and major element concentrations on 433 Eros: Evidence for an L- or LL-chondrite-like surface composition. *Meteoritics & Planetary Science*, *50*(3), 353–367.
Peplowski, P. N., Evans, L. G., Hauck, S. A., McCoy, T. J., Boynton, W. V., Gillis-Davis, J. J., … Stockstill-Cahill, K. R. (2011). Radioactive elements on Mercury's surface from MESSENGER: Implications for the planet's formation and evolution. *Science*, *333*(6051), 1850–1852.
Peplowski, P. N., Evans, L. G., Stockstill-Cahill, K., Lawrence, D. J., Goldsten, J. O., McCoy, T. J., … Weider, S. Z. (2014). Enhanced sodium abundance in Mercury's north polar region revealed by the MESSENGER Gamma-Ray Spectrometer. *Icarus*, *228*, 86–95.
Peplowski, P. N., Lawrence, D. J., Evans, L. G., Klima, R. L., Blewett, D. T., Goldsten, J. O., … Weider, S. Z. (2015). Constraints on the abundance of carbon in near-surface materials on Mercury: Results from the MESSENGER Gamma-Ray Spectrometer. *Planetary and Space Science*, *108*, 98–107.

Peplowski, P. N., Lawrence, D. J., Feldman, W. C., Goldsten, J. O., Bazell, D., Evans, L. G., … Weider, S. Z. (2015). Geochemical terranes of Mercury's northern hemisphere as revealed by MESSENGER neutron measurements. *Icarus*, *253*, 346–363.

Peplowski, P. N., Klima, R. L., Lawrence, D. J., Ernst, C. M., Denevi, B. W., Frank, E. A., … Solomon, S. C. (2016). Remote sensing evidence for an ancient carbon-bearing crust on Mercury. *Nature Geoscience*, *9*(4), 273–276.

Pernet-Fisher, J. F., Day, J. M. D., Howarth, G. H., Ryabov, V. V., & Taylor, L. A. (2017). Atmospheric outgassing and native-iron formation during carbonaceous sediment-basalt melt interactions. *Earth and Planetary Science Letters*, *460*, 201–212.

Pieters, C. M., & Noble, S. K. (2016). Space weathering on airless bodies. *Journal of Geophysical Research: Planets*, *121*, 1865–1884. https://doi.org/10.1002/2016JE005128

Pieters, C. M., Taylor, L. A., Noble, S. K., Keller, L. P., Hapke, B., Morris, R. V., … Wentworth, S. (2000). Space weathering on airless bodies: Resolving a mystery with lunar samples. *Meteoritics & Planetary Science*, *35*(5), 1101–1107.

Prettyman, T. H., Mittlefehldt, D. W., Yamashita, N., Lawrence, D. J., Beck, A. W., Feldman, W. C., … Russell, C. T. (2012). Elemental mapping by Dawn reveals exogenic H in Vesta's regolith. *Science*, *338*(6104), 242–246.

Prissel, T. C., Parman, S. W., & Head, J. W. (2016). Formation of the lunar highlands Mg-suite as told by spinel. *American Mineralogist*, *101*(7), 1624–1635.

Prockter, L. M., Ernst, C. M., Denevi, B. W., Chapman, C. R., Head, J. W., Fassett, C. I., … Massironi, M. (2010). Evidence for young volcanism on mercury from the third MESSENGER flyby. *Science*, *329*(5,992), 668–671.

Riner, M. A., & Lucey, P. G. (2012). Spectral effects of space weathering on Mercury: The role of composition and environment. *Geophysical Research Letters*, *39*, L12201. https://doi.org/10.1029/2012GL052065

Riner, M. A., Lucey, P. G., Desch, S. J., & McCubbin, F. M. (2009). Nature of opaque components on Mercury: Insights into a Mercurian magma ocean. *Geophysical Research Letters*, *36*, L02201. https://doi.org/10.1029/2008GL036128

Riner, M. A., McCubbin, F. M., Lucey, P. G., Talyor, G. J., & Gillis-Davis, J. J. (2010). Mercury surface composition: Integrating petrologic modeling and remote sensing data to place constraints on FeO abundance. *Icarus*, *209*(2), 301–313.

Robinson, M. S., & Taylor, G. J. (2001). Ferrous oxide in Mercury's crust and mantle. *Meteoritics & Planetary Science*, *36*(6), 841–847.

Ropp, R. C. (2013). *Encyclopedia of the alkaline Earth Compounds* (pp. 1216). Oxford, UK: Elsevier.

Rutherford, M. J., & Papale, P. (2009). Origin of basalt fire-fountain eruptions on Earth versus the Moon. *Geology*, *37*(3), 219–222.

Santos, A. R., Agee, C. B., McCubbin, F. M., Shearer, C. K., Burger, P. V., Tartèse, R., & Anand, M. (2015). Petrology of igneous clasts in Northwest Africa 7034: Implications for the petrologic diversity of the martian crust. *Geochimica et Cosmochimica Acta*, *157*, 56–85.

Sarma, B., Cramb, A. W., & Fruehan, R. J. (1996). Reduction of FeO in smelting slags by solid carbon: Experimental results. *Metallurgical and Materials Transactions B: Process Metallurgy and Materials Processing Science*, *27*(5), 717–730.

Sato, M., (1979). The driving mechanism for lunar pyroclastic eruptions inferred from the oxygen fugacity behavior of Apollo 17 orange glass. Presented at the Proceedings of the 10th lunar and Planetary Science Conference (pp. 311–325). Houston, TX.

Scaillet, B., Clemente, B., Evans, B. W., & Pichavant, M. (1998). Redox control of sulfur degassing in silicic magmas. *Journal of Geophysical Research*, *103*(B10), 23937–23949. https://doi.org/10.1029/98JB02301

Sehlke, A., & Whittington, A. G. (2015). Rheology of lava flows on Mercury: An analog experimental study. *Journal of Geophysical Research: Planets*, *120*, 1924–1955. https://doi.org/10.1002/2015JE004792

Self, S., Widdowson, M., Thordarson, T., & Jay, A. E. (2006). Volatile fluxes during flood basalt eruptions and potential effects on the global environment: A Deccan perspective. *Earth and Planetary Science Letters*, *248*(1–2), 518–532.

Sharp, Z. D., McCubbin, F. M., & Shearer, C. K. (2013). A hydrogen-based oxidation mechanism relevant to planetary formation. *Earth and Planetary Science Letters*, *380*, 88–97.

Singletary, S. J., & Grove, T. L. (2003). Early petrologic processes on the ureilite parent body. *Meteoritics & Planetary Science*, *38*(1), 95–108.

Solomon, S. C., McNutt, R. L. Jr., Gold, R. E., Acuña, M. H., Baker, D. N., Boynton, W. V., … Zuber, M. T. (2001). The MESSENGER mission to Mercury: scientific objectives and implementation. *Planetary and Space Science*, *49*(14-15), 1445–1465.

Stanley, B. D., Hirschmann, M. M., & Withers, A. C. (2011). CO_2 solubility in Martian basalts and Martian atmospheric evolution. *Geochimica et Cosmochimica Acta*, *75*(20), 5987–6003.

Stanley, B. D., Schaub, D. R., & Hirschmann, M. M. (2012). CO_2 solubility in primitive martian basalts similar to Yamato 980459, the effect of composition on CO_2 solubility of basalts, and the evolution of the martian atmosphere. *American Mineralogist*, *97*(11-12), 1841–1848.

Stockstill-Cahill, K. R., McCoy, T. J., Nittler, L. R., Weider, S. Z., & Hauck, S. A. II (2012). Magnesium-rich crustal compositions on Mercury: Implications for magmatism from petrologic modeling. *Journal of Geophysical Research*, *117*, E00L15. https://doi.org/10.1029/2012JE004140

Taylor, L. A., Pieters, C. M., Keller, L. P., Morris, R. V., & McKay, D. S. (2001). Lunar Mare Soils: Space weathering and the major effects of surface-correlated nanophase Fe. *Journal of Geophysical Research*, *106*(E11), 27985–27999. https://doi.org/10.1029/2000JE001402

Thomas, R. J., Rothery, D. A., Conway, S. J., & Anand, M. (2014a). Long-lived explosive volcanism on Mercury. *Geophysical Research Letters*, *41*, 6084–6092. https://doi.org/10.1002/2014GL061224

Thomas, R. J., Rothery, D. A., Conway, S. J., & Anand, M. (2014b). Mechanisms of explosive volcanism on Mercury: Implications from its global distribution and morphology. *Journal of Geophysical Research, Planets*, *119*, 2239–2254. https://doi.org/10.1002/2014JE004692

Thomas, R. J., Thomas, R., Cremonese, G., Rothery, D., Massironi, M., Re, C., … Anand, M. (2015). A cone on Mercury: Analysis of a residual central peak encircled by an explosive volcanic vent. *Planetary and Space Science*, *108*, 108–116.

Trail, D., Watson, E. B., & Tailby, N. D. (2011). The oxidation state of Hadean magmas and implications for early Earth's atmosphere. *Nature*, *480*(7375), 79–82.

Ulffmoller, F. (1990). Formation of native iron in sediment-contaminated magma: I. A case study of the Hanekammen Complex on Disko Island, West Greenland. *Geochimica et Cosmochimica Acta*, *54*(1), 57–70.

Ustunisik, G., Nekvasil, H., Lindsley, D. H., & McCubbin, F. M. (2015). Degassing pathways of Cl-, F-, H-, and S-bearing magmas near the lunar surface: Implications for the composition and Cl isotopic values of lunar apatite. *American Mineralogist*, *100*(8-9), 1717–1727.

Vander Kaaden, K. E., & McCubbin, F. M. (2015a). Exotic crust formation on Mercury: Consequences of a shallow, FeO-poor mantle. *Journal of Geophysical Research: Planets*, *120*, 195–209. https://doi.org/10.1002/2014JE004733

Vander Kaaden, K. E., McCubbin, F. M. (2015b). Sulfur solubility in silicate melts under highly reducing conditions relevant to Mercury. Presented at the Proceedings of the 46th Lunar and Planetary Science Conference (1040 pp.). Woodlands, TX: Lunar and Planetary Institute.

Vander Kaaden, K. E., & McCubbin, F. M. (2016). The origin of boninites on Mercury: An experimental study of the northern volcanic plains lavas. *Geochimica et Cosmochimica Acta*, *173*, 246–263.

Vander Kaaden, K. E., McCubbin, F. M., Nittler, L. R., Peplowski, P. N., Weider, S. Z., Frank, E. A., & McCoy, T. J. (2017). Geochemistry, mineralogy, and petrology of boninitic and komatiitic rocks on the Mercurian surface: Insights into the Mercurian mantle. *Icarus*, *285*, 155–168.

Vasavada, A. R., Paige, D. A., & Wood, S. E. (1999). Near-surface temperatures on Mercury and the Moon and the stability of polar ice deposits. *Icarus*, *141*(2), 179–193.

Vilas, F. (1988). Surface composition of Mercury from reflectance spectrophotometry. In F. Vilas, C. R. Chapman, & M. S. Matthews (Eds.), *Mercury* (pp. 59–76). Tucson, AZ: The University of Arizona Press.

Wadhwa, M. (2008). Redox conditions on small bodies, the Moon, and Mars. *Oxygen in the Solar System*, *68*, 493–510.

Walker, D., & Grove, T. (1993). Ureilite smelting. *Meteoritics*, *28*(5), 629–636.

Weider, S. Z., Nittler, L. R., Murchie, S. L., Peplowski, P. N., McCoy, T. J., Kerber, L., … Solomon, S. C. (2016). Evidence from MESSENGER for sulfur- and carbon-driven explosive volcanism on Mercury. *Geophysical Research Letters*, *43*, 3653–3661. https://doi.org/10.1002/2016GL068325

Weider, S. Z., Nittler, L. R., Starr, R. D., Crapster-Pregont, E. J., Peplowski, P. N., Denevi, B. W., … Solomon, S. C. (2015). Evidence for geochemical terranes on Mercury: Global mapping of major elements with MESSENGER's X-Ray Spectrometer. *Earth and Planetary Science Letters*, *416*, 109–120.

Weider, S. Z., Nittler, L. R., Starr, R. D., McCoy, T. J., & Solomon, S. C. (2014). Variations in the abundance of iron on Mercury's surface from MESSENGER X-Ray Spectrometer observations. *Icarus*, *235*, 170–186.

Wilson, L., & Head, J. W. (2017). Generation, ascent and eruption of magma on the Moon: New insights into source depths, magma supply, intrusions and effusive/explosive eruptions (Part 1: Theory). *Icarus*, *283*, 146–175.

Yoshioka, T., McCammon, C., Shcheka, S., & Keppler, H. (2015). The speciation of carbon monoxide in silicate melts and glasses. *American Mineralogist*, *100*(7), 1641–1644.

Zolotov, M. Y. (2011). On the chemistry of mantle and magmatic volatiles on Mercury. *Icarus*, *212*(1), 24–41.

Zolotov, M. Y., Sprague, A. L., Hauck, S. A. II, Nittler, L. R., Solomon, S. C., & Weider, S. Z. (2013). The redox state, FeO content, and origin of sulfur-rich magmas on Mercury. *Journal of Geophysical Research: Planets*, *118*, 138–146. https://doi.org/10.1029/2012JE004274